The dynamic core microbiome: structure, stability and resistance

Johannes R. Björk[1,5*], Robert B. O'Hara[2], Marta Ribes[3], Rafel Coma[4], and José M. Montoya[5*]

[1]University of Notre Dame, United States

[2]Biodiversity and Climate Research Centre, Frankfurt, Germany

[2]Department of Mathematical Sciences, NTNU, Trondheim, Norway

[3]Institute of Marine Sciences (ICM-CSIC), Barcelona, Spain

[4]Centre d'Estudis Avançats de Blanes (CEAB-CSIC), Blanes, Spain

[5]Theoretical and Experimental Ecology Station, CNRS-University Paul Sabatier, Moulis, France

[1]*rbjork@nd.edu (Corresponding author)*

[2]*bob.ohara@ntnu.no*

[3]*mribes@icm.csic.es*

[4]*coma@ceab.csic.es*

[5]*josemaria.montoyateran@sete.cnrs.fr (Corresponding author)*

May 12, 2017

Abstract

The long-term stability of microbiomes is crucial as the persistent occurrence of beneficial microbes and their associated functions ensure host health. Microbiomes are highly diverse and dynamic, but are they complex to the point of being impossible to understand? We present an approach that while embracing this complexity it allows to identifying meaningful patterns: the dynamic core microbiome. We study the structure, dynamics and stability of microbiomes belonging to six marine sponges sampled monthly over three years. We show that microbiome temporal stability is not determined by the diversity of their microbial assemblages, but by the abundance density of those microbes that conform their core microbiome. High-density cores confer hosts resistance against the establishment of occasional taxa to which sponges are constantly exposed through their filter-feeding activities. The core microbial interaction network consisted of complementary members interacting weakly with a dominance of commensal and amensal interactions that have likely coevolved to maintain host functionality and fitness.

Introduction

Microbes form intricate relationships with most animals and plants, with symbiosis postulated as one of the driving forces behind diversifications across the tree of life ([41]). Research on host-microbe symbiosis is typically restricted to highly specialized reciprocal interactions with one or a few microbes interacting with a single host, resulting in mutual benefits for the host and the microbe(s) ([21, 53]). However, more diverse and complex host-associated microbial communities (hereafter *microbiomes*) are increasingly found in different plant and animal species ([41]). This poses a challenge because the pairwise specificity, coevolution and reciprocity of host-microbe interactions might not explain the structure, dynamics and functioning of microbiomes. The mere existence of multiple microbes interacting with a host suggests that microbe-microbe interactions might also be an important driver regulating the overall composition and abundance of microbiomes and their associated ecosystem functions. The individually unique, but temporal stable microbiome of the human gut, for example, is likely to be regulated by interactions among its constituent members ([16]).

The diversity, complexity and highly dynamic nature of microbiomes makes them difficult to understand. We thus require approaches that embrace the complexity and dynamics of microbiomes but still allow identifying meaningful biological patterns. The quest for core microbiomes is a promising avenue ([80, 81, 69, 68, 1, 4, 28]). A temporal dimension has rarely been considered for determining the core microbiome ([7, 16, 17]). A core microbiome, broadly defined as a set of microbes consistently present over long periods of time is likely to have a large effect on the

development, health and functioning of its host. Studies on humans, for example, have revealed that several aspects of human health, including autoimmune disorders ([62, 64]), diabetes ([57]) and obesity ([33, 81]) can be linked to severe shifts in gut microbiome composition. Whether these disorders emerge as a consequence of perturbed core microbiomes still remains to be seen. Arguably, the long-term stability of the core microbiome is likely critical as the persistent occurrence of beneficial microbes and their associated functions ensure host health and well-being ([25, 35, 59, 10, 43]).

Despite the recent realizations that complex microbiomes pervade the tree of life, little is known about microbiome dynamics beyond humans. Here we study the structure, dynamics and stability of the microbiomes of six coexisting marine sponges (*Porifera*) belonging to different orders that were sampled over 36 consecutive months.

Sponges are key-species in marine coastal areas due to their filter-feeding activities. They regulate primary and secondary production by transferring energy between the pelagic and benthic zones ([23, 11]). Despite their constant influx of water, they maintain highly diverse, yet specific microbiomes with little intraspecific variation ([77]). As *Porifera* is a sister-group to all other multicellular animals ([71]), their associations with microbes likely represent the oldest extant form of animal-microbe symbiosis ([75, 27, 90]). The sponge hosts analyzed here correspond to two different groups that are shown to differ markedly in numerous traits, illustrating their dependence upon their associated microbes. The classification is based on the diversity and abundance of microbes they harbor – High and Low Microbial Abundance (HMA and LMA), respectively. This classification pervades host morphology and physiology: LMA hosts have an interior architecture fitted for pumping large volumes of water, whereas HMA hosts are morphologically adapted to harbor denser microbial assemblages within their tissue ([86, 66]). As a result, LMA hosts are more dependent on nutrient uptake from the water column ([29, 86, 66, 19, 37]), whereas HMA hosts rely more heavily on nutrients produced by their microbial symbionts ([19, 37, 60, 20, 18, 56]). These two sets of hosts provide an ideal system from which we can generalize whether the structure and temporal dynamics of complex microbiomes differs across hosts with different eco-evolutionary characteristics and lifestyles.

Our general aim is to understand the temporal dynamics of complex microbiomes. More specifically, we try to answer (i) what is the diversity and community structure of each core microbiome, and how does it differ from that of the many transient taxa passing through the host? (ii) what are the temporal dynamics and stability of each microbial taxa and their aggregated effect on the core microbiome? and (iii) what are the likely ecological processes that underpin the observed temporal dynamics and stability? We expect the answer to each of these questions to differ across hosts with different lifestyles (i.e., HMA vs. LMA hosts), reflecting their different dependency on their respective microbiomes. In particular, we expect the core microbiomes harboured by HMA hosts to be more diverse

and stable over time.

Results

Diversity and compositional overlap

We divided each microbiome into three different temporal assemblages based on the persistence of individual OTUs (Operational Taxonomic Units; hereafter *taxa*) over the 36 consecutive months. Core microbiomes consisted of taxa present in more than (or equal to) 70% of each time-series (i.e., persisting $\geq$ 26 months), whereas opportunistic assemblages comprised taxa present in less than (or equal to) 30% of each the time-series (i.e., persisting $\leq$ 11 months). The transient assemblages consisted of intermediately persistent taxa (i.e., those persisting between 12 and 25 months). We analyzed six microbiomes; three belonging to hosts classified as HMA (*Agelas oroides*, *Chondrosia reniformis*, *Petrosia ficiformis*) and three from hosts classified as LMA (*Axinella damicornis*, *Dysidea avara*, *Crambe crambe*) ([22, 15]).

Core microbiome diversity (species richness) only represented a small fraction (1.24%) of the overall diversity that resulted from the aggregation of all taxa found throughout the time-series, with a dominance of opportunistic taxa. HMA hosts harbored about 5 to 6 times more taxa in their core microbiomes than LMA hosts (Table 1). These taxa represented an important fraction of monthly diversity, particularly in HMA hosts, where opportunistic assemblages only had between 4 to 5 times more taxa than the core microbiomes. In contrast, LMA hosts harbored 19 to 25 times more opportunistic than core taxa (Table 1).

Compared to our null model that replicated each microbiome over time by randomly sample taxa from a regional pool consisting of all taxa found within the six microbiomes including the water column (Figure S3), we found that microbiome composition differed markedly across hosts (Figure 1) and lifestyles (HMA vs LMA) (Figure S1, with very little overlap among core microbiomes (Figure 2). The taxonomic profiles of the core microbiomes also differed between HMA and LMA hosts. The former harbored three dominant phyla that accounted for roughly half of their diversity. However, these hosts still kept their own individually unique taxonomic profiles by harboring other phyla, such as *Actinobacteria*, *Nitrospira*, *Spirochaetes* and *SAUL* (Figure 3). In stark contrast, the core microbiomes found within LMA hosts were largely dominated by taxa belonging to the phylum *Proteobacteria* (Figure 3).

Sponges are known to harbor certain taxa highly specific to the phylum Porifera (i.e., sponge-specific clusters) ([26, 72]). These taxa are only detected at very low abundances outside of the sponge host, e.g., in the sediment and seawater ([75, 74]). Some of these sponge-specific clusters are transmitted vertically, suggesting sponge-microbe

coevolution and cospeciation ([76]). We found that the core microbiomes of HMA hosts harbored a larger proportion of taxa that corresponded to sponge-specific clusters than LMA hosts (Table 2, Figure S2). We further found that these taxa had a higher average monthly abundance in the core microbiomes compared to the transient and opportunistic assemblages (Table S1). These results contrast with the expectations derived from the null model, where the proportion of taxa belonging to sponge-specific clusters and their average monthly abundances displayed opposite patterns, i.e., the proportion decreased while their average abundances increased from the cores to the opportunistic assemblages (Tables S2-S3). Overall, this suggests that a suite of non-random assembly processes, e.g., host selection of specific taxa and microbial interaction dynamics may be responsible for the observed patterns.

Temporal variability

We next analyzed temporal variability across microbiomes. Individual core and transient taxa were both more stable (measured by their coefficient of variation) and abundant than opportunistic taxa (Figure 4, Figures S4-S7). Temporal turnover is an intrinsic property of our definition of core microbiomes and transient and opportunistic assemblages. For example, as opportunistic taxa persist less than 30% of the total time-series, these assemblages are bound to heavily fluctuate in microbial composition. Nevertheless, in order to quantify the temporal turnover of each assemblage, we applied a newly developed measure that disentangles the two additive determinants of temporal turnover, i.e., change in total abundance and change in species composition ([70]). As expected, we found that core microbiomes were overall driven by changes in abundance, whereas transient and opportunistic assemblages were mainly governed by changes in microbial composition (Figures S8-S10).

The aggregated microbial relative abundance for each assemblage and host reveals two markedly different microbiome temporal dynamics (Figure 5). In the microbiomes of host *A. oroides*, *C. reniformis* and *C. crambe*, cores were very dense, i.e., they accounted for the majority of microbiome relative abundance. In contrast, the core microbiomes of host *D. avara*, *A. damicornis* and *P. ficiformis* were sparser, and instead transient and/or opportunistic assemblages dominated microbiome relative abundance (Figure 5, Table S3). The presence of abundant and transient taxa are likely to have a negative impact on the stability of the core microbiome (Figure 4, Figures S4-S7). We found that dense cores were more stable over time than sparse cores, measured as invariability (i.e., the inverse of variability) ([24]), both at the population and community level (Figure 5). This suggests that high-density cores conferred hosts a resistance against occasional taxa to increase in abundance.

Although we did not focus on measuring synchrony *per se*, it is interesting to note that the ratio of the two invariability measures reflect community-wide synchrony ([24]). Synchrony is linked to community stability, where

a larger diversity tends to increase the potential for species asynchrony, thus stabilizing community level properties ([34]).

Core dynamics and ecological interactions

We finally aimed to determine the relative importance of biotic interactions and environmental variability for core microbiome dynamics. We developed a Bayesian modeling framework assuming Gompertz population dynamics that decomposes temporal variation in microbial population abundances into contributions of interspecific and intraspecific interactions and environmental variability. Apart from ecological drift, environmental variability includes measured and unmeasured effects of both the host and the external environment acting on the host. In order to test if environmental factors had any effect on the analyzed microbiomes, we included in our model, several environmental covariates, such as water temperature, salinity, chlorophyll and nutrients.

As interspecific interactions require species to frequently co-occur, the many occasional taxa observed across our time-series, especially those occurring at high abundances are likely acting together with ecological drift as sources of stochastic noise. Our framework models Lotka-Volterra type of interactions, estimating the microbial interaction matrix where interaction coefficients correspond to the per capita influence of microbe j on the growth rate of microbe i. We used these interaction coefficients to determine and characterize core interaction networks.

We found that intraspecific interactions explained the largest proportion of variation, thus indicating that all core taxa, on average, experienced strong self-regulation (Figure 6A). The modelled environmental covariates only explained a small fraction of the relatively large proportion of variation explained by environmental variability (Figures S11-S16). We further found a marked difference between HMA and LMA hosts in terms of variation explained by interspecific interactions. In the core microbiomes of HMA hosts, interspecific interactions had a relatively large effect on the dynamics, while this type of interactions had a negligible effect in LMA hosts (Figure 6A). As a consequence, we analyzed the network structure of each HMA core microbiome. For those networks, we found that only a small fraction of the interspecific interactions among the possible ones were likely to occur (Figures S17-S18), resulting in low network connectance, with values ranging from 5 to 7%. These interactions were mostly very weak, with a skewed distribution of interaction strengths towards many weak and a few strong interactions in each core microbiome (Figures S19). Among the most probable interactions (Figures S18), we found largely unilateral interactions in the form of commensalism $\{+,0\}$ and amensalism $\{-,0\}$ (Figure 6B). Reciprocal interactions, such as cooperative $\{+,+\}$, competitive $\{-,-\}$ and exploitative $\{+,-\}$ interactions were exceptionally rare.

Each core interaction network had a mixture of positive and negative interactions, and nodes with high and low

degrees, i.e., the number of in- and out-going links (Figures 7-S20). As noted above, all HMA core microbiomes had a high proportion of taxa assigning to sponge-specific clusters. However, we did not observe that these taxa were more connected than other taxa within each core microbiome network.

Discussion

In order to increase our understanding of the processes that govern microbiome assembly, stability and functionality, it is critical to incorporate temporal dynamics. Recent studies have shown that microbiomes are examples of highly diverse dynamical systems. Most of these studies have focused on the human microbiome ([8, 17, 5, 12]), but a few studies have explored temporal dynamics in other animal-host systems ([7, 55]).

In contrast to the diversity-stability relationship ([40]), we did not observe an increase in stability with diversity (species richness). Instead, we found that temporal stability was associated with core microbiome abundance. In three hosts (two HMA and one LMA host), core microbiomes accounted for the majority of relative abundance, resulting in high-density cores. In the remaining three hosts (two LMA and one HMA host), the relative abundances of core microbiomes were similar or lower than that of the transient and/or opportunistic assemblages, resulting in low-density cores. Low-density cores showed larger variation over time than high-density cores, suggesting that core microbiome stability indeed was negatively affected by the presence of occasionally abundant taxa. In other words, high-density cores conferred hosts a resistance against occasional taxa to increase in abundance. Previous studies have shown that diversity confer ecosystems a resistance to the establishment of biological invasions ([30]). Our results suggest that it is not only diversity that determines invasion resistance, but also the dominance of the core microbiome in terms of its relative abundance. This could be responsible for the stability of host functioning, as in some cases, the abundance of common species, not species richness, is the main driver of ecosystem functioning ([89]).

High-density cores were found in sponge species that transmit commensal taxa vertically from adult to larvae offspring ([32, 82, 67]), whereas low-density cores correspond to sponge species with larvae deprived of microbes ([31, 61, 38]). Vertical transmission provides an evolutionary mechanism for preserving particular combinations of taxa, and their associated ecosystem functions ([79]). Vertical transmission thus underpins the observed temporal stability of high-density cores, and confers a high resistance against invasion and establishment of occasional taxa. Evidence from other ecological communities suggest that the arrival order of species affects community assembly and stability, resulting in priority effects ([9, 73]). The process of vertical inheritance of commensals likely has similar outcomes as classical priority effects. Moreover, as pathogenic taxa can use cooperative secretions that modify their

environment to enhance their growth and expansion ([52, 42]), it is reasonable to assume that commensals do too. We therefore hypothesize that the complementary set of taxa that are transmitted from adult to offspring preempt the host niche by fast reaching carrying capacity, while simultaneously modifying it in their favour. This will further inhibit the colonization of some taxa, while facilitating the establishment of others (e.g. horizontally selected taxa).

In agreement with the HMA-LMA dichotomy, the metabolic profiles of *P. ficiformis* and *C. crambe* match those of other HMA and LMA hosts, respectively ([45]). The low-density core of HMA host *P. ficiformis* was temporally variable but harbored a high diversity, whereof the majority could be assigned to sponge-specific clusters. In fact, this particular host harbored the highest proportion of sponge-specific taxa, suggesting that *P. ficiformis* displays HMA characteristics by means of horizontally selecting commensals from the water column. The innate immune defense of some sponge species is known to differentiate between pathogens, food bacteria and commensals in a manner similar to the adaptive immune system of vertebrates ([88, 85, 87, 78, 91, 14]). This finding indicates that sponge-specific clusters, although present in the water column and sediment as part of the rare biosphere ([84, 74]), represent taxa likely important for host functionality.

Other than density, species interactions and environmental stochasticity also have a strong effect on community dynamics and stability. In concert with studies on large free-living communities, we found that intraspecific interactions were an important determinant of abundance variability across core microbiomes ([50, 3, 39, 13]). However, while these studies showed that environmental stochasticity was the single most important determinant affecting dynamics, we found that the majority of temporal variation across core microbiomes was explained by intraspecific interactions. Moreover, our included environmental covariates only explained a small fraction of the relatively larger amount of variation explained by stochasticity. These differences are likely due to the fact that microbiomes reside inside a host, thus experiencing a reduced influence from the external environment acting on the host. More interestingly, we found that interspecific interactions explained a much larger proportion of temporal variation in the core microbiomes of HMA than LMA hosts. These interspecific interactions were similar, both in sign and strength. Theoretical results have shown that reciprocal interactions, such as exploitation $\{+/-\}$, cooperation $\{+/+\}$ and competition $\{-/-\}$ differ in their effects on community stability and ecosystem functioning ([46, 48, 47, 36, 63, 12, 49]), with communities consisting of a mixture of unilateral interactions being more stable than those with only reciprocal interactions ([49]). In concert, we found that HMA core microbiomes were characterized by unilateral interactions with similar degrees of commensalism $\{+, 0\}$ and amensalism $\{-, 0\}$. While the core microbiomes of hosts *A. oroides* and *C. reniformis* were largely dominated by commensal interactions, the core microbiome of host *P. ficiformis* had a higher frequency of amensalism. It was also the only core microbiome that displayed competitive interactions among its members, albeit

at very low frequencies. Asymmetric interaction signs and strengths are important for species coexistence and network stability ([6, 2]). In agreement, we observed skewed distributions of interaction strengths towards a few strong and many weak interactions.

Our study highlights the importance of defining core microbiomes temporally rather than cross-sectionally. Our results show that it is density and not diversity what primarily determines the stability of the sponge microbiome irrespective of hosts' eco-evolutionary characteristics and lifestyles, and that HMA core microbiomes consist of complementary commensals only interacting weakly and unilaterally among each other. We hypothesize that it is the constituent members of the core microbiome and their interactions that give rise to HMA characteristic functionality, regardless of these taxa being vertically inherited or horizontally selected. Our results further suggest that these interactions are a result of a mutual dependency between the microbes and the host, with both parties having the capacity to actively modify their interactions ([44]). The sponge host and its core commensals have likely coevolved in ways which allow for maintaining both functionality and fitness over ecological, and even evolutionary time scales.

Methods

Sponge collection

Sponge specimens from species *Agelas oroides*, *Chondrosia reniformis*, *Petrosia ficiformis*, *Axinella damicornis*, *Dysidea avara* and *Crambe crambe* were collected monthly from March 2009 until February 2012 close to the Islas Medas marine reserve in the NW Mediterranean Sea $42°3'0''N$, $3°13'0''E$ by SCUBA at depths between 10-15 m. The collected sponge species belong to six different orders, and represent common members of the Mediterranean benthic community. Each species were identified based on distinct morphological features. Replicates were carefully placed in separate plastic bottles and brought to the surface. Three replicates per sponge species were sampled and frozen in liquid nitrogen until DNA extractions.

DNA extraction and sequencing

16S rRNA gene sequences was PCR-amplified from 25 mg of sponge tissue per sample using the DNeasy tissue kit (Qiagen, Valencia, CA) and submitted the Research and Testing Laboratory (Lubbock, TX, USA) for gene amplicon pyrosequencing sequencing. Samples were amplified with primer 28F and amplicons were sequenced using Roche 454 Titanium chemistry, producing reads in the 5'→3' direction.

Analysis of sequencing data

454 reads were processed in mothur v.1.29.2 ([65]). Raw reads were pooled from replicates belonging to the same sponge species. Fasta, qual and flow files were extracted from binary sff files; sffinfo(…,flow=T). Flow files were then filtered based on barcodes to speed-up the proceeding de-noising process; trim.flow. Sequences were de-noised; shhh.flows(…, lookup= LookUp_Titanium.pat). The LookUp-file is necessary and specific to the 454 technology used. Next the barcode and primer sequences were removed together with sequences shorter than 200bp and/or contained homopolymers longer than 8bp; trim.seqs(…, pdiffs =2, bdiffs =1, maxhomop =8, minlength =200). In order to minimise computational effort, files were reduced to non identical sequences; unique.seqs. Non redundant sequences were aligned to SILVA 102 reference alignment with default kmer search and Needleman-Wunsch algorithm; align.seqs(…, flip =F). Non overlapping sequences were removed; screen.seqs(…, optimize= end, start= 1044, criteria = 95), in addition to empty columns that were introduced from the alignment process; filter.seqs(…,vertical =T, trump =.). Aligned sequences were reduced to non redundant sequences; unique.seqs. To further reduce amplification errors, less abundant sequences were binned to more abundant sequences if they were within 2bp of a difference; pre.cluster(…, diffs =2). Chimeric sequences were identified; chimera.uchime(…, dereplicate =T) and removed; remove.seqs. Sequences were classified using the RDP reference taxonomy; classify.seqs(…, template =trainset9_ 032012.pds.fasta, taxonomy =trainset9_ 032012.pds.tax, cutoff =80), and non bacterial lineages were removed; remove.lineage(…, taxon= Mitochondria-Chloroplast-Archaea-Eukaryota-unknown). We calculated pairwise distances between aligned sequences; dist.seqs(…, cutoff =0.050).

Due to an uneven sequence distribution across samples, we pooled all sequences from the three monthly replicates per host species, and because of plate effects in sequence counts, we sub-sampled 1500 sequences from each monthly host sample. This number corresponded to the average of the three lowest host-plate averages. This was followed by clustering sequences into OTUs defined at 97% similarity; classify.otu(…, label=0.030) and creating an OTU-table (.shared-file); make.shared(…, label=0.030). Beyond that, all analyses were conducted in R ([58]).

Identification of sponge-specific clusters

A representative sequence from each OTU was taxonomically assigned using a BLAST 62 search against a curated ARB-SILVA database containing 178 previously identified sponge-specific clusters (SC) ([72]). For each BLAST search, the 10 best hits were aligned to determine sequence similarities. The most similar OTU sequence to the respective reference sequence within the database was then assigned to an SC based on a 75% similarity threshold,

i.e., (i) a sequence was only assigned to any given SC if its similarity was higher to the members of the cluster than to sequences outside the cluster and (ii) if its similarity to the most similar sequence within the cluster was above 75%. A majority rule was applied in cases where the assignment of the most similar sequences was inconsistent, and the OTU sequence was only assigned to the SC if at least 60% of the reference sequences were affiliated with the cluster.

Null model

In order to assess whether random assembly processes from a species-rich regional pool generated empirical patterns in species diversity, relative abundance and compositional overlap across hosts, we created a simple null model that replicated each microbiome over the time-series. In our null model, a regional pool was created on a monthly basis by pooling all OTUs and their sequence counts from the corresponding month across hosts, including the water column. A "stochastic realization" was created for each host microbiome by randomly sample the same number of sequences present in each month from the corresponding monthly regional pool. This meant that OTUs were randomly sampled from each monthly regional pool in proportion to their abundance. We ran the null model 999 times for each host microbiome.

Temporal dynamics

Temporal turnover

We applied a newly developed measure of temporal turnover that describes the extent to which individual OTUs and consequently the microbiome changes over time ([70]. Importantly, this measure decomposes abundance fluctuations into two additive contributions of change due to microbiome composition and total abundance.

Total turnover D between times t and u, $(u > t)$ is defined as

$$D(t:u) = \sum_{i=1}^{S} d_i(t:u) = \sum_{i=1}^{S} \log\left(\frac{\lambda_{i,u}}{\lambda_{i,t}}\right) p_{i,t} \tag{1}$$

$$= -\sum_{i=1}^{S} \log\left(\frac{p_{i,t}}{p_{i,u}}\right) p_{i,t} + \left(\frac{\lambda_u}{\lambda_t}\right) \tag{2}$$

$$= D_1(p_t : p_u) + D_2(\lambda_t : \lambda_u) \tag{3}$$

where $\lambda_t = \sum_{i=1}^{S} \lambda_{i,t}$ represent the sum of the expected total abundance of each OTU in the microbiome. The expected abundance $\lambda_{i,t}, i = 1, 2, \ldots, S$ is unknown and therefore needs to be estimated from an observed time-series. $p_{i,t}$

represents the relative abundance of OTU i in time t and is calculated as $p_{i,t} = \left(\frac{\lambda_{i,t}}{\lambda_t}\right)$. As such, total turnover D can be decomposed into D_1 which is related to the amount of change in microbiome composition, and D_2 reflecting the amount of change in total abundance.

As noted above, the expected abundance needs to be estimated, thus we modelled each time-series of sequence counts $N_{i,t}$ assuming a Poisson distribution with a time varying mean $\lambda_{i,t}$

$$N_{i,t} \sim Pois(\lambda_{i,t}) \tag{4}$$

$$\log(\lambda_{i,t}) = \sum_{j=1}^{N_c} X_{t,k}\beta_{k,j} \tag{5}$$

where $X_{k,t}$ is a time-series of $k = 1, 2, \ldots, N_c$ environmental covariates, and $\beta_{k,j}$ is the corresponding regression coefficient that needs to be estimated. We included temperature, salinity, chlorophyll, bacterial cell density, nitrite (NO_2), ammonia (NH_4), and phosphate (PO_4) as the N_c environmental covariates. All covariates where standardized to have zero-mean and unit variance.

Temporal invariability

We applied two newly developed measures of temporal stability, i.e. invariability ([24]) in order to assess the stability at the population (i.e. for each OTU) and community level (i.e. for opportunistic and transient assemblages and the core microbiome), respectively.

Invariability at the population and community level is defined as

$$I_{pop} = \frac{1}{\left(\sum_i \frac{\widehat{N}_i}{\widehat{N}_{tot}} CV(N_i)\right)^2} = \frac{(\widehat{N}_{tot})^2}{\left(\sum_i \sqrt{Var(N_i)^2}\right)} \tag{6}$$

$$I_{com} = \frac{1}{CV(N_{tot})^2} = \frac{(\widehat{N}_{tot})^2}{Var(N_{tot})} \tag{7}$$

where the total-abundance of a community N_{tot} is the sum of each OTUs' abundance as $N_{tot} = \sum_{i=1}^{S} N_i$, and the $\widehat{N}_{tot}$ and $\widehat{N}_i$ denotes their respective averages.

Interestingly, these two measures are connected. The ratio of I_{pop} and I_{com} equals community-wide synchrony

$$\frac{I_{pop}}{I_{com}} = \frac{Var(N_{tot})}{\sum_i \sqrt{Var(N_i)^2}} \tag{8}$$

with 0 and 1 for perfectly asynchronous and synchronous communities, respectively. This implies that $I_{pop} \leq I_{com}$, and that the equality $I_{pop} = I_{com}$ represents a perfectly synchronous community.

Core dynamics and ecological interactions

We developed a multivariate first-order autoregressive model assuming Gompertz population dynamics based on [50] for modeling core dynamics and to infer interactions between core OTUs from time-series of sequence counts.

Process model If we denote $n_{i,t}*$ as the expectation of $n_{i,t}$ which is the natural logarithm of the observed time-series $N_{i,t}$, then on the natural logarithmic scale we have the expected number of sequences belonging to core OTU i in time t within any given host species described by

$$n_{i,t}*|n_{i,t-1} = n_{i,t-1} + r_i\left[1 - \sum_{j=1}^{S} \frac{\alpha_{i,j} n_{j,t-1}}{k_i}\right] + \sum_{j=1}^{N_c} X_{t,k}\beta_{k,j} + \varepsilon_{i,t} \tag{9}$$

$$t = 2, 3, \ldots, T; k = 1, 2, \ldots, N_c$$

where we assume $r_i \sim \mathcal{N}(0, 10)$ and $K_i \sim Exp(1)$. The coefficients measuring each OTUs' response the $k-th$ environmental covariate are assumed $\beta_{k,j} \sim \mathcal{N}(0, 100)$. The residual variance $\varepsilon_{i,t}$ representing apart from ecological drift, un-modelled host effects and the effects of the un-modelled external environmental acting on the host, are assumed to be serially independent and normally distributed. We included temperature, salinity, chlorophyll, bacterial cell density, nitrite (NO_2), ammonia (NH_4) and phosphate (PO_4) as the N_c environmental covariates potentially affecting the residing microbiomes. All covariates where standardized to have zero-mean and unit variance. Furthermore, we used a latent variable approach to model correlations between taxa (see [83]).

Observation model The time-series of sequence counts are modeled as a Poisson process, where $y_{i,t}$ denotes the number of sequences of core taxa i in time t

$$y_{i,t} = Pois(\lambda_{i,t}) \tag{10}$$

$$\log \lambda_{t,i} = n_{i,t} + \log N_t + \mu N_t \tag{11}$$

$$n_{i,t} = \mathcal{MVN}(n_{i,t}*, \sigma_i^2) \tag{12}$$

where N_t and $\mu N_t \sim \mathcal{N}(0, 100)$ both are offsets representing the total abundance in time t.

We used Gibbs Variable Selection (GVS) ([54]) method in order to constrain the model to only use interspecific interaction coefficients $\alpha_{i,j}$ for which there are strong support in the data. This is achieved by introducing a binary indicator variable $\gamma_{i,j}$ for $i \neq j$, and assuming $\gamma_{i,j} \sim Bernoulli(p)$, such that $\gamma_{i,j} = 1$ when OTU j is included in the dynamics of OTU i, and $\gamma_{i,j} = 0$, otherwise. Where there is low support for $\alpha_{i,j}$ in the data, $\gamma_{i,j} = 0$ and the corresponding interaction is excluded from the model. When $\gamma_{i,j} = 1$, $\alpha_{i,j}$ is freely estimated from the data. p represent our prior belief about how many of all interspecific interaction are actually realized. We chose value of 0.1, which means that we did not expect more than 10% of all possible interspecific interactions to take place.

Variance partitioning Following [50] and [51], the total variance V_i affecting the dynamics of core OTU i can be decomposed into additive sources reflecting interspecific interactions, intraspecific interactions (i.e. density-dependence), and environmental variability (i.e. measured environmental covariates and residual variance)

$$V_i = \overbrace{\left[\frac{r_i}{K_i}\right]^2 \sum_{j \neq i} v_{j,j}\alpha_{i,j}^2}^{\text{Interspecific interactions}} + \overbrace{\left[\frac{r_i}{K_i}\right]^2 v_{i,i}}^{\text{Intraspecific interactions}} + \overbrace{\sum_{i=1}^{N_c} \beta_{i,q}^2 + \varepsilon_i}^{\text{Environmental variability}} \quad (13)$$

where $v_{i,i}$ represent the stationary variance for n_i (Equation 11), $\beta_{i,k}^2$ the variance attributable to each k covariate, and ε_i correspond to residual variance. As a consequence of Equation 13, the proportion of variation attributed to e.g. interspecific interactions can be calculated as

$$\sigma_{i_{Inter}}^2 = \left\{\left[\frac{r_i}{K_i}\right]^2 \sum_{j \neq i} v_{j,j}\alpha_{i,i}^2\right\} \Big/ V_i \quad (14)$$

To determine and characterize core microbiome networks, we analyzed the interaction and sign structure of the posterior probability distribution for the interaction coefficient $\alpha_{i,j}$. Because $\alpha_{i,j}$ is a probability distribution, it contains the probability of OTU j having a per capita effect on the growth of OTU i (interaction strength), and vice versa. Using all information in $\alpha_{i,j}$, we constructed core networks for each HMA host as means of visualizing the most 'credible' network structure. This was done by mapping the posterior average number of links onto α_{ij}, and in doing so, extracting the posterior average number of links with the highest probability of non-zero interactions. This was done by custom-written R scripts. As a way of validating the structure of each core network, we compared the connectance of each network to the posterior average connectance for $\alpha_{i,j}$ for each host. The networks were plotted using the *igraph* package in R v.3.2.1.

Finally, we used Markov chain Monte Carlo (MCMC) simulation methods through JAGS in R using the *runjags* package to sample from the joint posterior distribution of all the model parameters. We ran 10 independent chains with dispersed initial values for 5e6 iterations, discarding the first 2e6 samples of each chain as burn-in and thinned the remainder to every 50-th sample. We evaluated convergence of model parameters by visually inspecting trace and density plots. In addition, to ensure good mixing of $\alpha_{i,j}$ we calculated the number of jumps $\gamma_{i,j}$ made between its two states, 0 and 1.

Acknowledgements

J.M.M. was supported by the French Laboratory of Excellence Project 'TULIP' (ANR-10-LABX-41; ANR-11-IDEX-002-02) and by a Region Midi-Pyrenees Project (CNRS 121090) and R.C and M.R (CGL2010-18466), and by a grant from the Catalan Government (2009SGR142). J.R.B was supported by an FPI Fellowship from the Spanish Government (BES-2011-049043).

References

[1] Tracy D. Ainsworth, Lutz Krause, Thomas Bridge, Gergely Torda, Jean-Baptise Raina, Martha Zakrzewski, Ruth D. Gates, Jacqueline L. Padilla-Gamino, Heather L. Spalding, Celia Smith, Erika S. Woolsey, David G. Bourne, Pim Bongaerts, Ove Hoegh-Guldberg, and William Leggat. The coral core microbiome identifies rare bacterial taxa as ubiquitous endosymbionts. *The ISME Journal*, 9(10):2261–2274, 2015.

[2] Stefano Allesina and Si Tang. Stability criteria for complex ecosystems. *Nature*, 483(7388):205–208, 2012.

[3] Pablo Almaraz and Daniel Oro. Size-mediated non-trophic interactions and stochastic predation drive assembly and dynamics in a seabird community. *Ecology*, 92(10):1948–1958, 2011.

[4] Carmen Astudillo-García, James J. Bell, Nicole S. Webster, Bettina Glasl, Jamaluddin Jompa, Jose M. Montoya, and Michael W. Taylor. Evaluating the core microbiota in complex communities: A systematic investigation. *Environmental Microbiology*, 19(4):1450–1462, 2017.

[5] Fredrik Backhed, Josefine Roswall, Yangqing Peng, Qiang Feng, Huijue Jia, Petia Kovatcheva-Datchary, Yin Li, Yan Xia, Hailiang Xie, Huanzi Zhong, Muhammad Tanweer Khan, Jianfeng Zhang, Junhua Li, Liang Xiao, Jumana Al-Aama, Dongya Zhang, Ying Shiuan Lee, Dorota Kotowska, Camilla Colding, Valentina Tremaroli,

Ye Yin, Stefan Bergman, Xun Xu, Lise Madsen, Karsten Kristiansen, Jovanna Dahlgren, and Wang Jun. Dynamics and stabilization of the human gut microbiome during the first year of life. *Cell Host and Microbe*, 17(5):690–703, 2015.

[6] Jordi Bascompte and Pedro Jordano. Plant-Animal Mutualistic Networks: The Architecture of Biodiversity. *Annual Review of Ecology, Evolution, and Systematics*, 38(2007):567–593, 2007.

[7] Johannes R. Björk, C. Díez-Vives, Rafel Coma, Marta Ribes, and José M. Montoya. Specificity and temporal dynamics of complex bacteria-sponge symbiotic interactions. *Ecology*, 94(12):2781–2791, 2013.

[8] Gregory J. Caporaso, Christian L. Lauber, William A. Walters, Donna Berg-Lyons, Catherine A. Lozupone, Peter J. Turnbaugh, Noah Fierer, and Rob Knight. Global patterns of 16S rRNA diversity at a depth of millions of sequences per sample. *Proceedings of the National Academy of Sciences of the United States of America*, 108:4516–22, 2011.

[9] Jonathan M. Chase. Stochastic community assembly causes higher biodiversity in more productive environments. *Science*, 328(5984):1388–91, 2010.

[10] Ilseung Cho and Martin J. Blaser. The human microbiome: at the interface of health and disease. *Nature Reviews Genetics*, 13(4):260–270, 2012.

[11] Martina Coppari, Andrea Gori, Núria Viladrich, Luca Saponari, Antonio Canepa, Jordi Grinyó, Alejandro Olariaga, and Sergio Rossi. The role of Mediterranean sponges in benthic–pelagic coupling processes: Aplysina aerophoba and Axinella polypoides case studies. *Journal of Experimental Marine Biology and Ecology*, 477(April):57–68, 2016.

[12] Katharine Z. Coyte, Jonas Schluter, and Kevin R. Foster. The ecology of the microbiome: Networks, competition, and stability. *Science*, 350(6261):663–666, 2015.

[13] Elizabeth E. Crone. Contrasting effects of spatial heterogeneity and environmental stochasticity on population dynamics of a perennial wildflower. *Journal of Ecology*, 104(2):281–291, 2016.

[14] Sandie M. Degnan. The surprisingly complex immune gene repertoire of a simple sponge, exemplified by the NLR genes: A capacity for specificity? *Developmental and Comparative Immunology*, 48(2):269–274, 2015.

[15] Patrick M. Erwin, Rafel Coma, Paula López-Sendino, Eduard Serrano, and Marta Ribes. Stable symbionts across the HMA-LMA dichotomy: low seasonal and interannual variation in sponge-associated bacteria from taxonomically diverse hosts. *FEMS Microbiology Ecology*, 91(910):fiv115, 2015.

[16] Jeremiah J. Faith, Janaki L. Guruge, Mark Charbonneau, Sathish Subramanian, Henning Seedorf, Andrew L. Goodman, Jose C. Clemente, Rob Knight, Andrew C. Heath, Rudolph L. Leibel, Michael Rosenbaum, and Jeffrey I. Gordon. The long-term stability of the human gut microbiota. *Science*, 341(6141):1237439, 2013.

[17] Gilberto E. Flores, J. Gregory Caporaso, Jessica B. Henley, Jai Ram Rideout, Daniel Domogala, John Chase, Jonathan W. Leff, Yoshiki Vázquez-Baeza, Antonio Gonzalez, Rob Knight, Robert R. Dunn, and Noah Fierer. Temporal variability is a personalized feature of the human microbiome. *Genome biology*, 15(12):531, 2014.

[18] Christopher J. Freeman, Cole G. Easson, and David M. Baker. Metabolic diversity and niche structure in sponges from the Miskito Cays, Honduras. *PeerJ*, 2:e695, 2014.

[19] Christopher J. Freeman and Robert W. Thacker. Complex interactions between marine sponges and their symbiotic microbial communities. *Limnology and Oceanography*, 56(5):1577–1586, 2011.

[20] Christopher J. Freeman, Robert W. Thacker, David M. Baker, and Marilyn L. Fogel. Quality or quantity: is nutrient transfer driven more by symbiont identity and productivity than by symbiont abundance? *The ISME Journal*, 7(6):1116–25, 2013.

[21] Rosario Gil, Beatriz Sabater-Muñoz, Amparo Latorre, Francisco J. Silva, and Andrés Moya. Extreme genome reduction in Buchnera spp.: toward the minimal genome needed for symbiotic life. *Proceedings of the National Academy of Sciences of the United States of America*, 99(7):4454–4458, 2002.

[22] Volker Gloeckner, Markus Wehrl, Lucas Moitinho-Silva, Christine Gernert, Peter Schupp, Joseph R Pawlik, Niels L Lindquist, Dirk Erpenbeck, Gert Wörheide, and Ute Hentschel. The HMA-LMA Dichotomy Revisited: an Electron Microscopical Survey of 56 Sponge Species. *The Biological bulletin*, 227(1):78–88, 2014.

[23] Jasper M De Goeij, Dick Van Oevelen, Mark J.A. Vermeij, Ronald Osinga, Jack J Middelburg, Anton F P M De Goeij, and Wim Admiraal. Surviving in a Marine Desert: The Sponge Loop Retains Resources Within Coral Reefs. *Science*, 342(October):108–110, 2013.

[24] Bart Haegeman, Jean-François Arnoldi, Shaopeng Wang, Claire de Mazancourt, José M. Montoya, and Michel Loreau. Resilience, invariability, and ecological stability across levels of organization. *bioRxiv*, 2016.

[25] Amber L. Hartman, Denver M. Lough, Dinesh K. Barupal, Oliver Fiehn, Thomas Fishbein, Michael Zasloff, and Jonathan A. Eisen. Human gut microbiome adopts an alternative state following small bowel transplantation. *Proceedings of the National Academy of Sciences*, 106(40):17187–17192, 2009.

[26] Ute Hentschel, Jörn Hopke, Matthias Horn, B. Anja, Michael Wagner, Jörg Hacker, S. Bradley, Anja B. Friedrich, and Bradley S. Moore. Molecular Evidence for a Uniform Microbial Community in Sponges from Different Oceans Molecular Evidence for a Uniform Microbial Community in Sponges from Different Oceans. *Applied and Environmental Microbiology*, 68(9):4431–4440, 2002.

[27] Ute Hentschel, Jörn Piel, Sandie M. Degnan, and Michael W. Taylor. Genomic insights into the marine sponge microbiome. *Nature Reviews Microbiology*, 10(9):641–654, 2012.

[28] Alejandra Hernandez-Agreda, Ruth D. Gates, and Tracy D. Ainsworth. Defining the Core Microbiome in Corals' Microbial Soup. *Trends in Microbiology*, 25(2):125–140, 2017.

[29] Eroteida Jiménez and Marta Ribes. Sponges as a source of dissolved inorganic nitrogen: Nitrification mediated by temperate sponges. *Limnology and Oceanography*, 52(3):948–958, 2007.

[30] Theodore A. Kennedy, Shahid Naeem, Katherine M. Howe, Johannes M.H. Knops, David Tilman, and Peter Reich. Biodiversity as a barrier to ecological invasion. *Nature*, 417(6889):636–638, 2002.

[31] E. Lepore, M. Sciscioli, M. Gherardi, and L. Scalera Liaci. The ultrastructure of the mature oocyte and the nurse cells of the ceractinomorpha *Petrosia ficiformis*. *Cahiers De Biologie Marine*, 36:15–20, 1995.

[32] C. Levi and P. Levi. Embryogenese de *Chondrosia reniformis* (Nardo), demosponge ovipare, et transmission des bacteries symbiotiques. *Ann Sci Nat Zool*, 18:367–380, 1976.

[33] Ruth E. Ley, Peter J. Turnbaugh, S. Klein, and Jeffrey I. Gordon. Microbial ecology: human gut microbes associated with obesity. *Nature*, 444(7122):1022–3, 2006.

[34] Michel Loreau. *From populations to ecosystems: theoretical foundations for a new ecological synthesis*. Monographs in population biology. Princeton University Press, 2010.

[35] Catherine A. Lozupone, Jesse I. Stomabaugh, Jeffery I. Gordon, Janet K. Jansson, and Rob Knight. Diversity, stability and resilience of the human gut microbiota. *Nature*, 489(7415):220–230, 2012.

[36] Miguel Lurgi, Daniel Montoya, and Jose M. Montoya. The effects of space and diversity of interaction types on the stability of complex ecological networks. *Theoretical Ecology*, 9(1):3–13, 2016.

[37] Manuel Maldonado, Marta Ribes, and Duyl van Fleur C. Chapter three - Nutrient Fluxes Through Sponges: Biology, Budgets, and Ecological Implications. In *Advances in Sponge Science: Physiology, Chemical and Microbial Diversity, Biotechnology*, volume 62 of *Advances in Marine Biology*, pages 113–182. Academic Press, 2012.

[38] Manuel Maldonado and Ana Riesgo. Gametogenesis, embryogenesis, and larval features of the oviparous sponge *Petrosia ficiformis* (Haplosclerida, Demospongiae). *Marine Biology*, 156(10):2181–2197, 2009.

[39] Carlos Martorell and Robert P. Freckleton. Testing the roles of competition, facilitation and stochasticity on community structure in a species-rich assemblage. *Journal of Ecology*, 102(1):74–85, 2014.

[40] Kevin S McCann. The diversity-stability debate. *Nature*, 405(May):228–233, 2000.

[41] Margaret McFall-Ngai, Michael G. Hadfield, Thomas C.G. Bosch, Hannah V. Carey, Tomislav Domazet-Lošo, Angela E. Douglas, Nicole Dubilier, Gerard Eberl, Tadashi Fukami, Scott F. Gilbert, Ute Hentschel, Nicole King, Staffan Kjelleberg, Andrew H. Knoll, Natacha Kremer, Sarkis K Mazmanian, Jessica L. Metcalf, Kenneth Nealson, Naomi E Pierce, John F. Rawls, Ann Reid, Edward G. Ruby, Mary Rumpho, Jon G. Sanders, Diethard Tautz, and Jennifer J. Wernegreen. Animals in a bacterial world, a new imperative for the life sciences. *Proceedings of the National Academy of Sciences*, 110(9):3229–3236, 2013.

[42] Luke McNally, Mafalda Viana, and Sam P. Brown. Cooperative secretions facilitate host range expansion in bacteria. *Nature communications*, 5:4594, 2014.

[43] Bayan Missaghi, Herman Barkema, Karen Madsen, and Subrata Ghosh. Perturbation of the Human Microbiome as a Contributor to Inflammatory Bowel Disease. *Pathogens*, 3(3):510–527, 2014.

[44] Lucas Moitinho-Silva, Cristina Diez-Vives, Giampiero Batani, Ana IS Esteves, Martin T. Jahn, and Torsten Thomas. Integrated metabolism in sponge-microbe symbiosis revealed by genome-centered metatranscriptomics. *The ISME Journal*, 2017.

[45] Teresa Morganti, Rafel Coma, Gitai Yahel, and Marta Ribes. Trophic niche separation facilitates co-existence of high and low microbial abundance sponges is revealed by in situ study of carbon and nitrogen fluxes. *Limnology and Oceanography*, In press.

462 [46] Akihiko Mougi and Michio Kondoh. Diversity of Interaction Types and Ecological Community Stability. *Sci-*
463 *ence*, 337(6092):349–351, 2012.

464 [47] Akihiko Mougi and Michio Kondoh. Adaptation in a hybrid world with multiple interaction types: a new
465 mechanism for species coexistence. *Ecological Research*, 29(2):113–119, 2014.

466 [48] Akihiko Mougi and Michio Kondoh. Stability of competition–antagonism–mutualism hybrid community and the
467 role of community network structure. *Journal of Theoretical Biology*, 360:54–58, 2014.

468 [49] Akihiko Mougi and Michio Kondoh. Food-web complexity, meta-community complexity and community stabil-
469 ity. *Scientific Reports*, 6(24478), 2016.

470 [50] Crispin M. Mutshinda, Robert B. O'Hara, and Ian P. Woiwod. What drives community dynamics? *Proceedings*
471 *of the Royal Society B*, 276(1669):2923–2929, 2009.

472 [51] Crispin M. Mutshinda, Robert B. O'Hara, and Ian P. Woiwod. A multispecies perspective on ecological impacts
473 of climatic forcing. *Journal of Animal Ecology*, 80(1):101–107, 2011.

474 [52] Teresa Nogueira, Daniel J. Rankin, Marie Touchon, François Taddei, Sam P. Brown, and Eduardo P C Rocha.
475 Horizontal Gene Transfer of the Secretome Drives the Evolution of Bacterial Cooperation and Virulence. *Current*
476 *Biology*, 19(20):1683–1691, 2009.

477 [53] Spencer V. Nyholm and Margaret J. McFall-Ngai. The winnowing: Establishing the squid-vibrio symbiosis.
478 *Nature Reviews Microbiology*, 2(8):632–642, 2004.

479 [54] Robert B. O'Hara and Mikko J. Sillanpää. A review of bayesian variable selection methods: What, how and
480 which. *Bayesian Analysis*, 4(1):85–118, 2009.

481 [55] D. W. Pitta, S. Kumar, B. Vecchiarelli, L. D. Baker, J. D. Ferguson, N. Thomsen, D. J. Shirley, and K. Bittinger.
482 Temporal dynamics in the ruminal microbiome of dairy cows during the transition period. *Journal of Animal*
483 *Science*, 92(9):4014–4022, 2014.

484 [56] Ericka Poppell, Jeremy Weisz, Lori Spicer, Andrew Massaro, April Hill, and Malcolm Hill. Sponge heterotrophic
485 capacity and bacterial community structure in high- and low-microbial abundance sponges. *Marine Ecology*,
486 35(4):414–424, 2014.

[57] Junjie Qin, Yingrui Li, Zhiming Cai, Shenghui Li, Jianfeng Zhu, Fan Zhang, Suisha Liang, Wenwei Zhang, Yuanlin Guan, Dongqian Shen, Yangqing Peng, Dongya Zhang, Zhuye Jie, Wenxian Wu, Youwen Qin, Wenbin Xue, Junhua Li, Lingchuan Han, Donghui Lu, Peixian Wu, Yali Dai, Xiaojuan Sun, Zesong Li, Aifa Tang, Shilong Zhong, Xiaoping Li, Weineng Chen, Ran Xu, Mingbang Wang, Qiang Feng, Meihua Gong, Jing Yu, Yanyan Zhang, Ming Zhang, Torben Hansen, Gaston Sanchez, Jeroen Raes, Gwen Falony, Shujiro Okuda, Mathieu Almeida, Emmanuelle LeChatelier, Pierre Renault, Nicolas Pons, Jean-Michel Batto, Zhaoxi Zhang, Hua Chen, Ruifu Yang, Weimou Zheng, Songgang Li, Huanming Yang, Jian Wang, S. Dusko Ehrlich, Rasmus Nielsen, Oluf Pedersen, Karsten Kristiansen, and Jun Wang. A metagenome-wide association study of gut microbiota in type 2 diabetes. *Nature*, 490(7418):55–60, 2012.

[58] R Core Team. *R: A Language and Environment for Statistical Computing*. R Foundation for Statistical Computing, Vienna, Austria, 2016.

[59] David A Relman. The human microbiome: ecosystem resilence and health. *Nutr Rev*, 70(Suppl 1):1–12, 2013.

[60] Marta Ribes, Eroteida Jiménez, Gitai. Yahel, Paula López-Sendino, Beatriz Diez, Ramon Massana, J.H. Sharp, and Rafel Coma. Functional convergence of microbes associated with temperate marine sponges. *Environmental Microbiology*, 14(5):1224–1239, 2012.

[61] Ana Riesgo and Manuel Maldonado. Differences in reproductive timing among sponges sharing habitat and thermal regime. *Invertebrate Biology*, 127(4):357–367, 2008.

[62] June L. Round and Sarkis K. Mazmanian. The gut microbiota shapes intestinal immune responses during health and disease. *Nat Rev Immunol*, 9(5):313–323, 2009.

[63] Alix M.C. Sauve, Colin Fontaine, and Elisa Thébault. Structure-stability relationships in networks combining mutualistic and antagonistic interactions. *Oikos*, 123(3):378–384, 2014.

[64] Jose U. Scher and Steven B. Abramson. The microbiome and rheumatoid arthritis. *Nat Rev Rheumatol*, 7(10):569–578, 2011.

[65] Patrick D. Schloss, Sarah L. Westcott, Thomas Ryabin, Justine R. Hall, Martin Hartmann, Emily B. Hollister, Ryan A. Lesniewski, Brian B. Oakley, Donovan H. Parks, Courtney J. Robinson, Jason W. Sahl, Blaz Stres, Gerhard G. Thallinger, David J. Van Horn, and Carolyn F. Weber. Introducing mothur: Open-source, platform-

513 independent, community-supported software for describing and comparing microbial communities. *Applied and*
514 *Environmental Microbiology*, 75(23):7537–7541, 2009.

515 [66] Marie Lise Schläppy, Sandra I. Schöttner, Gaute Lavik, Marcel M.M. Kuypers, Dirk de Beer, and Friederike
516 Hoffmann. Evidence of nitrification and denitrification in high and low microbial abundance sponges. *Marine*
517 *Biology*, 157(3):593–602, 2010.

518 [67] Susanne Schmitt, Hilde Angermeier, Roswitha Schiller, Niels Lindquist, and Ute Hentschel. Molecular microbial
519 diversity survey of sponge reproductive stages and mechanistic insights into vertical transmission of microbial
520 symbionts. *Applied and Environmental Microbiology*, 74(24):7694–7708, 2008.

521 [68] Susanne Schmitt, Ute Hentschel, and Michael W. Taylor. Deep sequencing reveals diversity and community
522 structure of complex microbiota in five Mediterranean sponges. *Hydrobiologia*, 687(1):341–351, 2012.

523 [69] Ashley Shade and Jo Handelsman. Beyond the Venn diagram: the hunt for a core microbiome. *Environmental*
524 *Microbiology*, 14(1):4–12, 2012.

525 [70] Hideyasu Shimadzu, Maria Dornelas, and Anne E. Magurran. Measuring temporal turnover in ecological com-
526 munities. *Methods in Ecology and Evolution*, 6(12):1384–1394, 2015.

527 [71] Paul Simion, Hervé Philippe, Denis Baurain, Muriel Jager, Daniel J. Richter, Arnaud Di Franco, Béatrice Roure,
528 Nori Satoh, Éric Quéinnec, Alexander Ereskovsky, Pascal Lapébie, Erwan Corre, Frédéric Delsuc, Nicole King,
529 Gert Wörheide, and Michaël Manuel. A Large and Consistent Phylogenomic Dataset Supports Sponges as the
530 Sister Group to All Other Animals. *Current Biology*, 2017.

531 [72] Rachel L. Simister, Peter Deines, Emmanuelle S. Botté, Nicole S. Webster, and Michael W. Taylor. Sponge-
532 specific clusters revisited: A comprehensive phylogeny of sponge-associated microorganisms. *Environmental*
533 *Microbiology*, 14(2):517–524, 2012.

534 [73] Fukami Tadashi. Historical Contingency in Community Assembly: Integrating Niches, Species Pools, and Pri-
535 ority Effects. *Annual Review of Ecology, Evolution, and Systematics*, 46(1):1–23, 2015.

536 [74] Michael W. Taylor, Peter Tsai, Rachel L. Simister, Peter Deines, Emmanuelle Botte, Gavin Ericson, Susanne
537 Schmitt, and Nicole S Webster. 'Sponge-specific' bacteria are widespread (but rare) in diverse marine environ-
538 ments. *The ISME Journal*, 7:438–443, 2013.

[75] Micheal W Taylor, Regina Radax, D Stegar, and M Wagner. Sponge-associated microorganisms: evolution, evology, and biotechnological potential. *Microbiology and Molecular Biology Reviews*, 71(2):295–347, 2007.

[76] Robert W Thacker and Christopher J. Freeman. Chapter two - Sponge–Microbe Symbioses: Recent Advances and New Directions. In *Advances in Sponge Science: Physiology, Chemical and Microbial Diversity, Biotechnology*, volume 62 of *Advances in Marine Biology*, pages 57–111. Academic Press, 2012.

[77] Torsten Thomas, Lucas Moitinho-Silva, Miguel Lurgi, Johannes R Björk, Cole Easson, Carmen Astudillo-García, Julie B Olson, Patrick M Erwin, Susanna López-Legentil, Heidi Luter, et al. Diversity, structure and convergent evolution of the global sponge microbiome. *Nature Communications*, 7, 2016.

[78] Torsten Thomas, Doug Rusch, Matt Z. DeMaere, Pui Yi Yung, Matt Lewis, Aaron Halpern, Karla B. Heidelberg, Suhelen Egan, Peter D. Steinberg, and Staffan Kjelleberg. Functional genomic signatures of sponge bacteria reveal unique and shared features of symbiosis. *The ISME Journal*, 4(12):1557–1567, 2010.

[79] John N. Thompson. *The geographic mosaic of coevolution*. University of Chicago Press, 2005.

[80] Matthias H. Tschöp, Philip Hugenholtz, and Christopher L. Karp. Getting to the core of the gut microbiome. *Nature biotechnology*, 27(4):344–346, 2009.

[81] Peter J. Turnbaugh, Micah Hamady, Tanya Yatsunenko, Brandi L. Cantarel, Alexis Duncan, Ruth E. Ley, Mitchell L. Sogin, William J Jones, Bruce A Roe, Jason P. Affourtit, Michael Egholm, Bernard Henrissat, Andrew C. Heath, Rob Knight, and Jeffrey I. Gordon. A core gut microbiome in obese and lean twins. *Nature*, 457(7228):480–484, 2009.

[82] María J. Uriz, Turon Xavier, and Becerro Mikel A. Morphology and Ultrastructure of the Swimming Larvae of *Crambe crambe* (Demospongiae, Poecilosclerida). *Invertebrate Biology*, 120(4):295–307, 2001.

[83] David I. Warton, F. Guillaume Blanchet, Robert B. O'Hara, Otso Ovaskainen, Sara Taskinen, Steven C. Walker, and Francis K C Hui. So Many Variables: Joint Modeling in Community Ecology. *Trends in Ecology and Evolution*, 30:1–14, 2015.

[84] Nicole S. Webster, Michael W. Taylor, Faris Behnam, Sebastian Lücker, Thomas Rattei, Stephen Whalan, Matthias Horn, and Michael Wagner. Deep sequencing reveals exceptional diversity and modes of transmission for bacterial sponge symbionts. *Environmental Microbiology*, 12(8):2070–2082, 2010.

[85] Markus Wehrl, Michael Steinert, and Ute Hentschel. Bacterial uptake by the marine sponge Aplysina aerophoba. *Microbial Ecology*, 53(2):355–365, 2007.

[86] Jeremy B. Weisz, Niels Lindquist, and Christopher S. Martens. Do associated microbial abundances impact marine demosponge pumping rates and tissue densities? *Oecologia*, 155(2):367–376, 2008.

[87] Matthias Wiens, Michael Korzhev, Sanja Perović-Ottstadt, Bérengère Luthringer, David Brandt, Stefanie Klein, and Werner E.G. Müller. Toll-like receptors are part of the innate immune defense system of sponges (Demospongiae: Porifera). *Molecular Biology and Evolution*, 24(3):792–804, 2007.

[88] C. R. Wilkinson. Microbial associations in sponges. III. Ultrastructure of the in situ associations in coral reef sponges. *Marine Biology*, 49(2):177–185, 1978.

[89] Rachael Winfree, Jeremy W. Fox, Neal M. Williams, James R. Reilly, and Daniel P. Cariveau. Abundance of common species, not species richness, drives delivery of a real-world ecosystem service. *Ecology Letters*, 18(7):626–635, 2015.

[90] Zongjun Yin, Maoyan Zhu, Eric H. Davidson, David J. Bottjer, Fangchen Zhao, and Paul Tafforeau. Sponge grade body fossil with cellular resolution dating 60 Myr before the Cambrian. *Proceedings of the National Academy of Sciences*, 112(12):E1453–E1460, 2015.

[91] Benedict Yuen, Joanne M. Bayes, and Sandie M. Degnan. The characterization of sponge nlrs provides insight into the origin and evolution of this innate immune gene family in animals. *Molecular Biology and Evolution*, 31(1):106–120, 2014.

583 # Tables and Figures

Table 1: Microbiome diversity by temporal assemblage

	HMA			LMA		
	A. oroides	*C. reniformis*	*P. ficiformis*	*A. damicornis*	*D. avara*	*C. crambe*
Core	45 38.4 ± 11.7	33 27.4 ± 11.1	40 32.1 ± 12.3	8 6.7 ± 2.1	6 6.4 ± 2	8 6.4 ± 2.3
Transient	90 41.3 ± 14.4	54 26.4 ± 12.5	140 67.9 ± 30.8	31 12.7 ± 5.9	44 21.4 ± 7.4	41 17.7 ± 6.2
Opportunistic	2658 140 ± 77.7	2436 129.9 ± 66.7	2580 141.4 ± 30.2	2443 126.8 ± 78.1	2763 126.3 ± 42.8	3465 160.1 ± 60.4
Total biome	2793	2523	2760	2482	2813	3514

Notes: For each assemblage, the first row displays the total number of unique taxa, while the second row shows the monthly average (± SD) number of coexisting taxa. The last row shows the total number of taxa present in each microbiome.

Table 2: Percentage of taxa within each assemblage and host assigning to sponge-specific clusters.

	HMA			LMA		
	A. oroides	*C. reniformis*	*P. ficiformis*	*A. damicornis*	*D. avara*	*C. crambe*
Core	42.2	45.6	60	25	0	12.5
Transient	43.3	40.7	47.1	25.8	9.1	9.8
Opportunistic	22.8	33.9	35.6	22.2	9.5	11.8

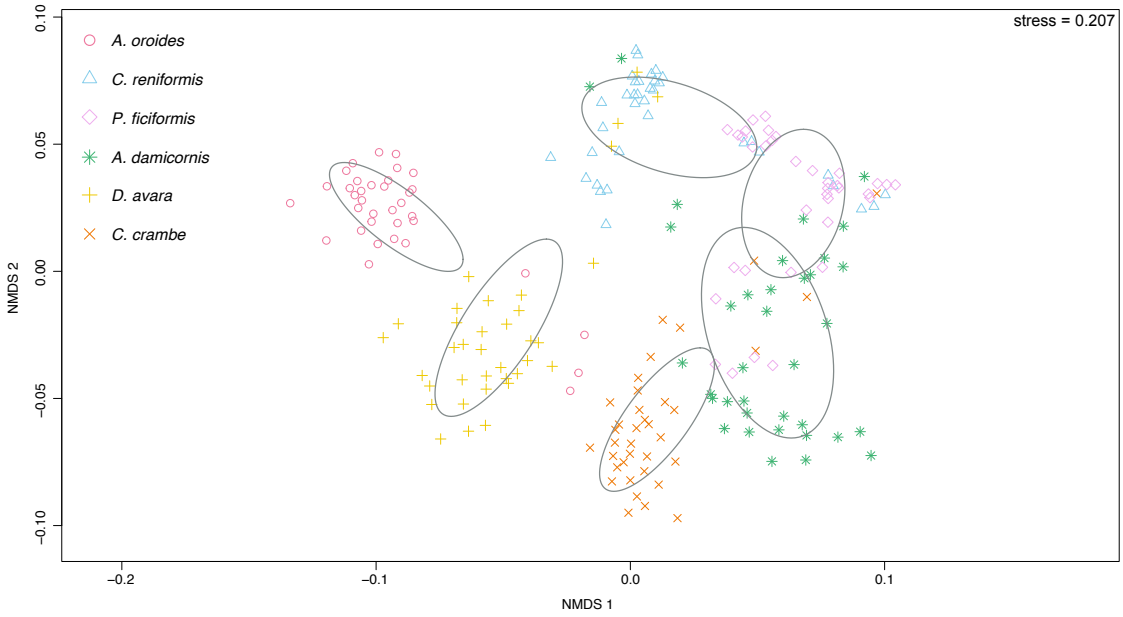

Figure 1: Microbiome compositional similarity across hosts and months. Non-metric multidimensional scaling (NMDS) calculated from Jaccard distances among all 36 monthly samples for each host. Colors and shapes denote all monthly samples from a given host species. Host samples are surrounded by an ellipse showing the 95% confidence interval around monthly samples. Red circles: *A. oroides*, blue triangles: *C. reniformis*, pink diamonds: *P. ficiformis*, green stars: *A. damicornis*, yellow crosses (+): *D. avara*, and orange crosses (×): *C. crambe*. ANOSIM: R=0.767, P<0.001

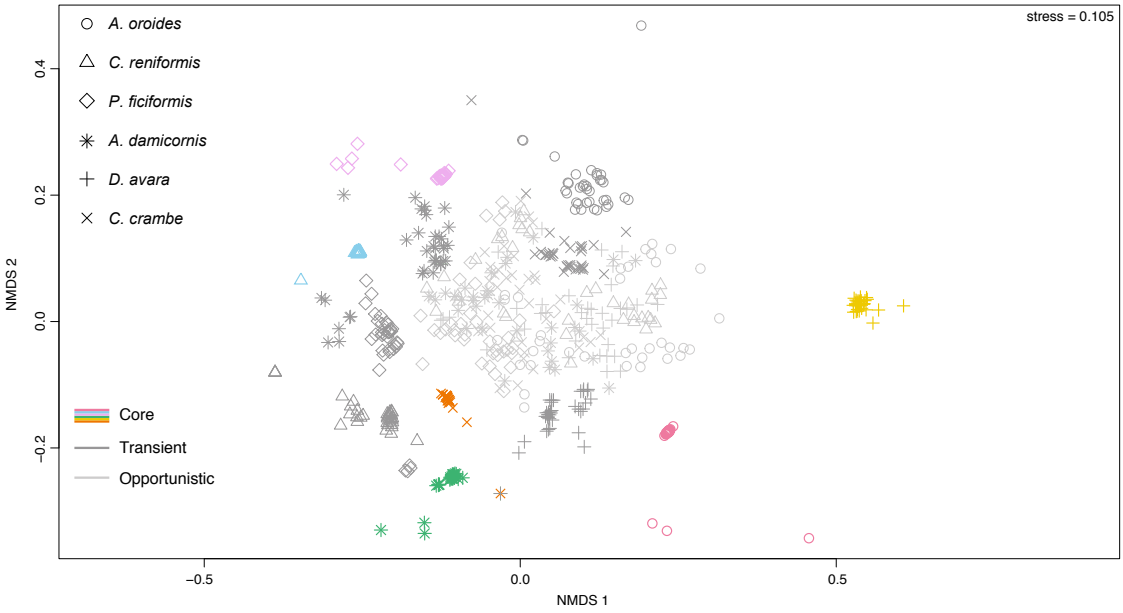

Figure 2: Microbiome compositional similarity across hosts and assemblages. Non-metric multidimensional scaling (NMDS) calculated from Jaccard distances among monthly samples for each host and assemblage. Colors and shapes denote all monthly samples from a given host and assemblage, respectively. Different shapes for each host species; circles: *A. oroides*, triangles: *C. reniformis*, diamonds: *P. ficiformis*, stars: *A. damicornis*, crosses (+): *D. avara*, crosses (×): *C. crambe*. Different colors for each core microbiome; red: *A. oroides*, blue: *C. reniformis*, pink: *P. ficiformis*, green: *A. damicornis*, yellow: *D. avara*, and orange: *C. crambe*. Dark gray denotes transient and light gray opportunistic assemblages, respectively.

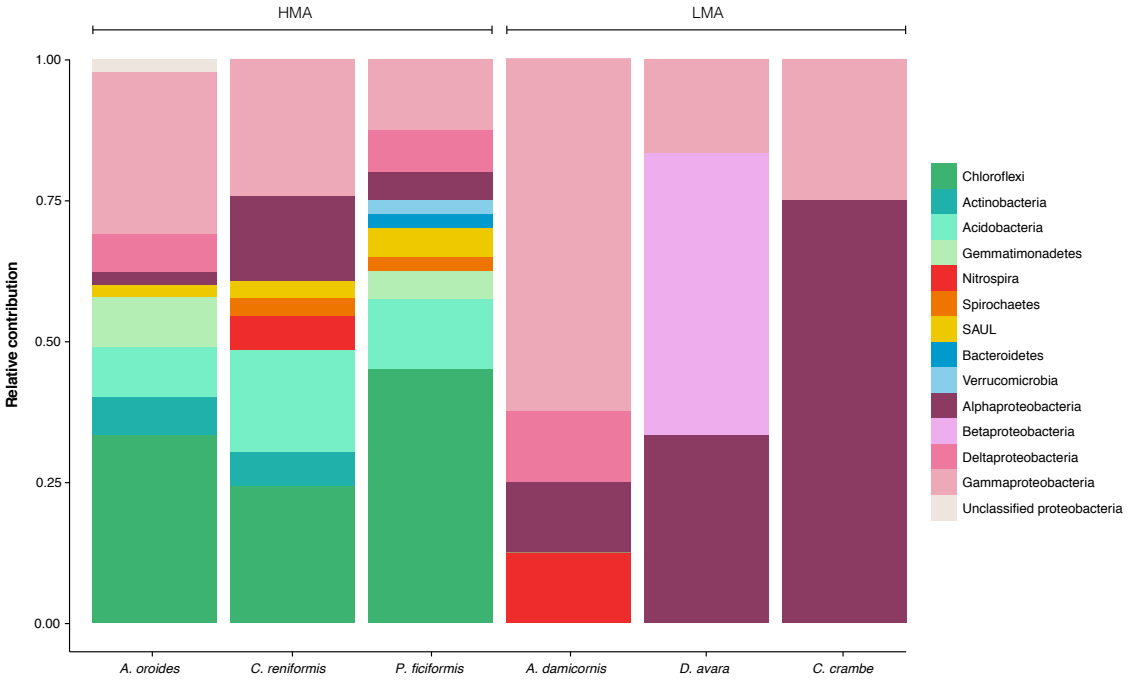

Figure 3: Taxonomic profiles of core microbiomes across hosts. Taxonomic classification at the phylum level of core taxa and their relative contribution to species richness for each core microbiome. The core microbiomes of HMA hosts harboured a larger taxonomic diversity than those of LMA hosts.

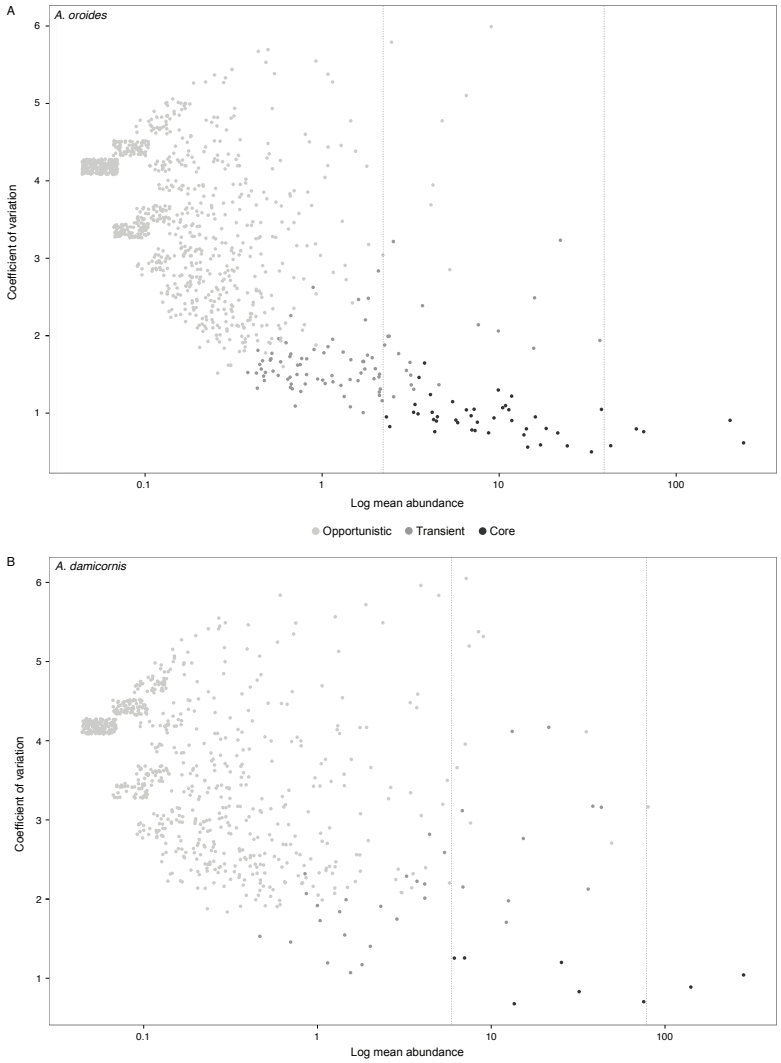

Figure 4: Abundance-stability relationship across microbiomes. The relationship between coefficient of variation (CV) and (log) mean abundance of individual taxa for host *A. oroides* (panel A) and host *A. damicornis* (panel B). Overlaying points have been separated by adding jitter (random noise) of 0.1 in both y and x direction. Opportunistic, transient and core taxa are each shown by an increasing grey scale. Individual core and transient taxa are generally more stable (Kruskal-Wallis test: H =2198, df=2, P<0.001 two-tailed; Dunn's post-hoc test with bonferroni correction; P <0.001) and abundant (Kruskal-Wallis test: H =1694, df= 2, P<0.001; Dunn's post-hoc test with bonferroni correction; P< 0.001 two-tailed) than opportunistic taxa. The gray dashed vertical lines mark a potentially critical area by which core microbiome temporal stability can be predicted. If there are only a few abundant and occasional taxa relative to the number of core taxa, stability is predicted to be high (*A. oroides*, panel A), whereas if there are many abundant and occasional taxa compared to the number of core taxa, stability is predicted to be low (*A. damicronis*, panel B). See Figures S4-S7 for the remaining hosts.

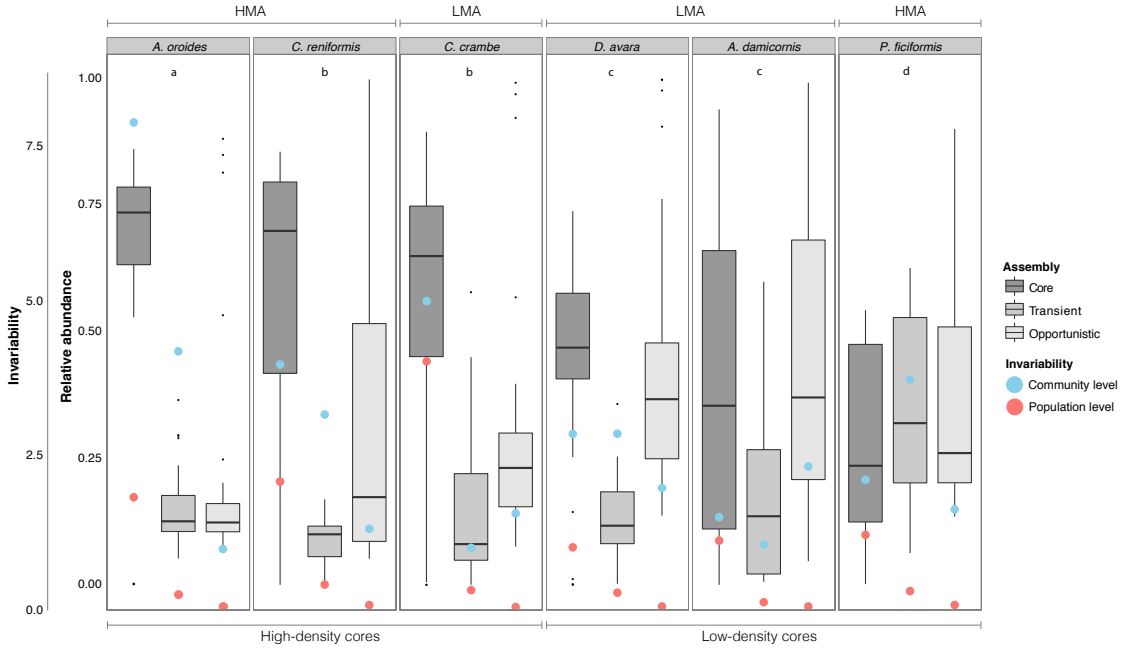

Figure 5: The contribution of assemblage type to microbiome abundance and its aggregated stability. The inner y-axis shows the contribution of the aggregated microbial relative abundance for each assemblage and host. Each box shows the median including the first and third quartiles (the 25^{th} and 75^{th} percentiles), representing temporal variation. The outer y-axis shows invariability (i.e., the inverse of variability) at the community (blue dots) level and population (red dots) for each assemblage and host. It is interesting to note that community-wide synchrony increases as the two dots approach each other. The figure is ordered from the highest to the lowest in terms of core density. Lowercase letters denote different significant scenarios (Dunn's post-hoc test for Kruskal-Wallis rank sum test (see Table S4 for more details). a: the core microbiome was significantly different from the transient and opportunistic assemblages, but transient and opportunistic assemblages were not significantly different from each other. b: all assemblages were significantly different. c: the core microbiome and the opportunistic assemblage were not significantly different, but the core microbiome and transient assemblage, and the transient and the opportunistic assemblage were significantly different from each other. d: no significant differences between any assemblages. What emerged was three high-density (scenario a & b), and three low-density (scenario c & d) cores, respectively.

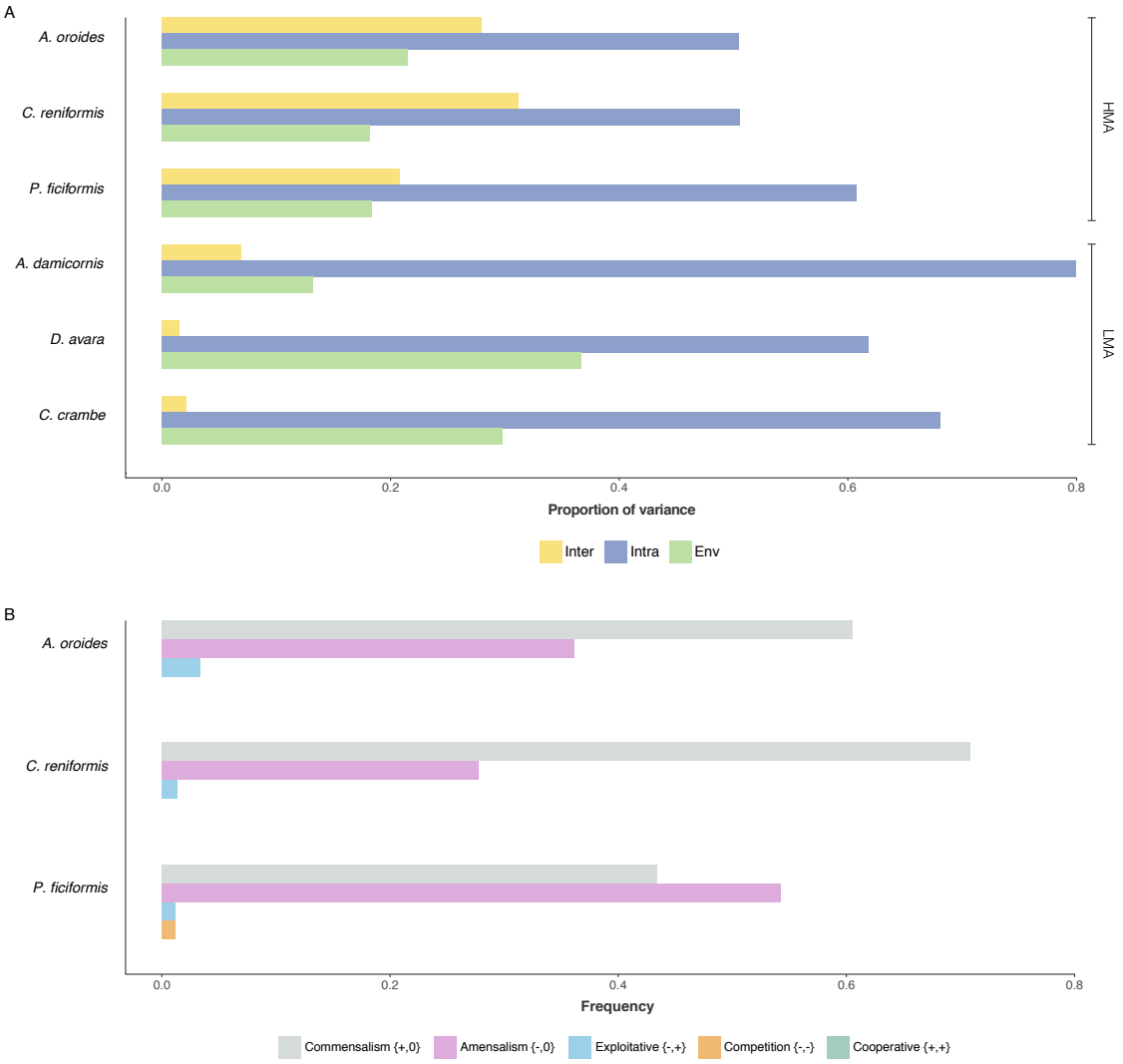

Figure 6: Processes explaining temporal variation in core microbial population abundances and the frequency of different interspecific interactions inferred from the HMA core microbiomes. Panel A shows the relative contribution of inter- and intraspecific (i.e. density-dependence) interactions and environmental variability to temporal variation in microbial population abundances across core microbiomes. In all hosts, core microbiome dynamics were mainly driven by intraspecific interactions (i.e. density-dependence). While core microbiomes were relatively equally affected by environmental variability, an important driver of the dynamics in HMA cores were interspecific interactions which was almost negligible in LMA cores. Panel B shows the relative frequency of all possible interaction types within HMA cores. Commensalism $\{+,0\}$ and amensalism $\{-,0\}$ were the most frequent interaction types across HMA cores. Competitive $\{-,-\}$ and exploitative $\{+,-\}$ interactions were exceptionally rare. Noteworthy, cooperative interactions $\{+,+\}$ was never inferred.

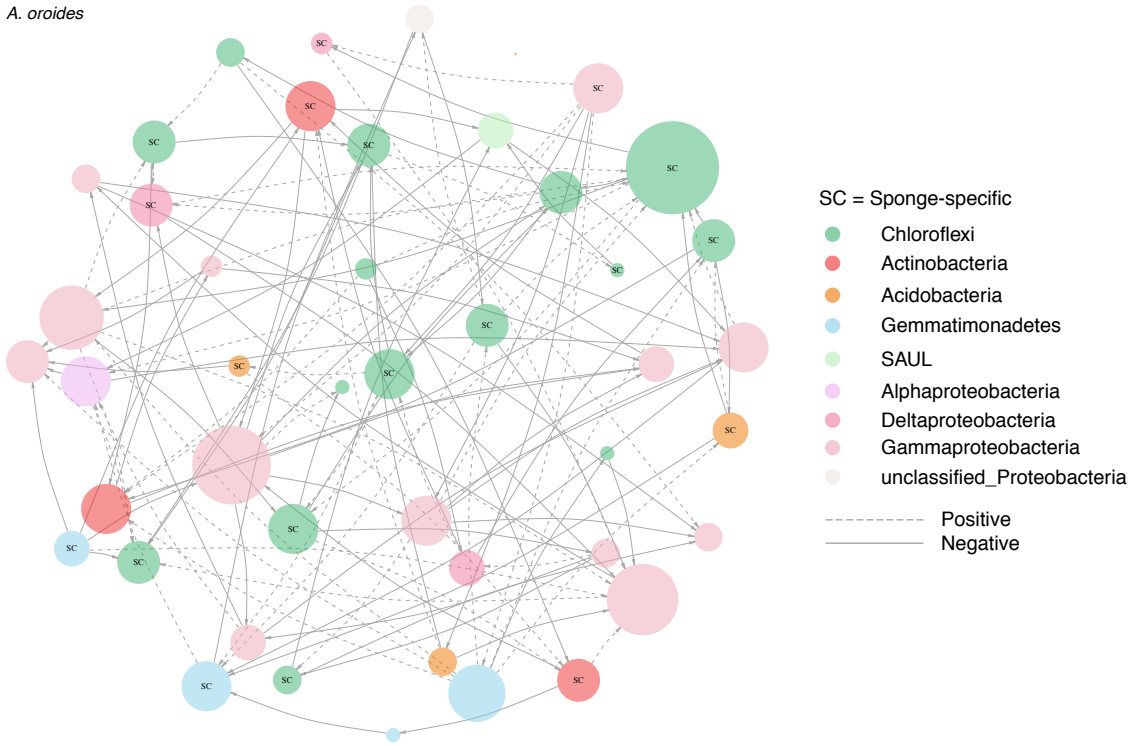

Figure 7: The core microbiome network of HMA host *A. oroides*. Nodes represent core taxa and links their inferred ecological interactions. Node size is scaled to their degree (i.e. in and out-going links). Colors correspond to different bacterial phyla and dash and solid lines represent positive and negative interactions, respectively. Nodes marked with SC correspond to taxa assigning to sponge-specific clusters. See Figure S20 for the remaining two HMA hosts.

Supplementary information

Table S1: Median (including 1^{st} and 3^{rd} quartiles) of average monthly abundances of taxa assigning to sponge-specific clusters shown for each assemblage and host

		HMA			LMA		
		A. oroides	*C. reniformis*	*P. ficiformis*	*A. damicornis*	*D. avara*	*C. crambe*
Core	1^{st} Qu.	6.7	6.6	4.2	29.2	0	1.8
	Median	**11.3**	**19.8**	**6.7**	**50.3**	**0**	**16.5**
	3^{rd} Qu.	19.2	32.8	13.8	71.5	0	39.0
Transient	1^{st} Qu.	0.6	1.1	1.0	3.1	0.6	1.0
	Median	**1.0**	**1.6**	**1.7**	**3.9**	**0.8**	**2.1**
	3^{rd} Qu.	2.3	3.1	2.5	5.2	1.2	33.9
Opportunistic	1^{st} Qu.	0.0	0.0	0.0	0.0	0.0	0.0
	Median	**0.0**	**0.0**	**0.0**	**0.0**	**0.0**	**0.1**
	3^{rd} Qu.	0.1	0.1	0.1	0.1	0.1	0.1

Table S2: Percentage (mean ± SD) of taxa belonging to sponge-specific clusters across assemblages within each hosts' "stochastic realisation".

	HMA			LMA		
	A. oroides	*C. reniformis*	*P. ficiformis*	*A. damicornis*	*D. avara*	*C. crambe*
Core	48.5 ± 0.21	48.6 ± 0.20	50.9 ± 0.22	48.6 ± 0.19	50.8 ± 0.23	48.2 ± 0.20
Transient	30.1 ± 1.6	29.8 ± 1.6	30.2 ± 1.8	29.7 ± 1.6	30.2 ± 1.7	29.8 ± 1.6
Opportunistic	2.9 ± 0.1	2.8 ± 0.1	3.4 ± 0.1	2.8 ± 0.1	3.3 ± 0.1	2.8 ± 0.1

Note: Mean ± SD were calculated from 999 permutations of the null model.

Table S3: Median (including 1^{st} and 3^{rd} quartiles) (mean ± SD) of the average monthly abundance of taxa assigning to sponge-specific clusters across assemblages within each hosts' "stochastic realisation".

		HMA			LMA		
		A. oroides	*C. reniformis*	*P. ficiformis*	*A. damicornis*	*D. avara*	*C. crambe*
Core	1^{st} Qu.	1.8 ± 0.2	1.7 ± 0.2	1.4 ± 0.1	1.8 ± 0.2	1.4 ± 0.2	1.9 ± 0.2
	Median	**2.6 ± 0.2**	**2.5 ± 0.2**	**1.9 ± 0.1**	**2.6 ± 0.2**	**2.1 ± 0.2**	**2.6 ± 0.2**
	3^{rd} Qu.	3.4 ± 0.2	3.3 ± 0.2	2.7 ± 0.2	3.3 ± 0.2	3.0 ± 0.2	3.4 ± 0.2
Transient	1^{st} Qu.	3.2 ± 0.3	3.1 ± 0.2	2.4 ± 0.2	3.2 ± 0.2	2.4 ± 0.2	3.3 ± 0.2
	Median	**4.4 ± 0.3**	**4.3 ± 0.3**	**3.4 ± 0.2**	**4.4 ± 0.3**	**3.6 ± 0.2**	**4.5 ± 0.3**
	3^{rd} Qu.	5.9 ± 0.4	5.8 ± 0.3	4.7 ± 0.3	5.8 ± 0.4	5.1 ± 0.3	6.0 ± 0.4
Opportunistic	1^{st} Qu.	16.0 ± 1.0	15.4 ± 1.0	11.5 ± 0.8	15.6 ± 1.1	11.2 ± 0.8	16.3 ± 1.1
	Median	**20.2 ± 1.2**	**20.0 ± 1.2**	**17.3 ± 1.1**	**20.0 ± 1.2**	**17.1 ± 1.0**	**20.3 ± 1.3**
	3^{rd} Qu.	23.7 ± 1.4	23.6 ± 1.4	21.9 ± 1.2	23.8 ± 1.5	24.8 ± 1.3	24.2 ± 1.4

Note: Mean ± SD were calculated from 999 permutations of the null model.

Table S4: Mean rank sums for relative abundance across assemblages and hosts. For each host, a Kruskal-Wallis rank sum test was computed to test for differences between assemblages. *A. oroides*: H=40.103, df=2, P<0.001 two-tailed, *C. reniformis*: H=31.222, df=2, P<0.001 two-tailed, *C. crambe*: H=40.696, df=2, P<0.001 two-tailed *D. avara*: H=48.474, df=2, P<0.001 two-tailed, *A. damicornis*: H=17.747, df=2, P<0.001 two-tailed; *P. ficiformis*: H=3.567, df=2, P=0.168 two-tailed. If there was a significant difference, Dunn's post-hoc test for pairwise comparisons with bonferroni correction was used.

	HMA			LMA		
	A. oroides	*C. reniformis*	*P. ficiformis*	*A. damicornis*	*D. avara*	*C. crambe*
Core	81.47	74.33	78.33	73.06	59.32	46.50
Transient	40.15	33.17	31.25	25.17	37.11	59.28
Opportunistic	41.88	56.00	53.92	65.28	67.07	57.72
	a	b	b	c	c	d

Note: The lowercase letters indicate different significant scenarios (see Figure 5 in main text). a: the core microbiome was significantly different from the transient and opportunistic assemblages, but transient and opportunistic assemblages were not significantly different from each other. b: all assemblages were significantly different. c: the core microbiome and the opportunistic assemblage were not significantly different, but the core microbiome and transient assemblage, and the transient and the opportunistic assemblage were significantly different from each other. d: no significant differences between any assemblages. What emerged was three high-density (scenario a & b), and three low-density (scenario c & d) cores, respectively.

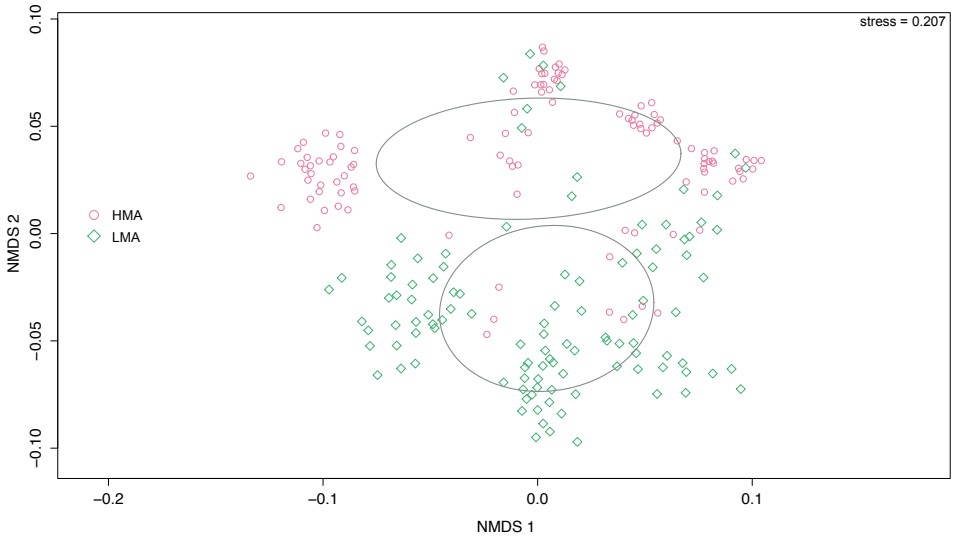

Figure S1: Microbiome compositional similarity across hosts and lifestyles. Non-metric multidimensional scaling (NMDS) calculated on Jaccard distances among monthly samples for each host lifestyle (i.e., HMA and LMA). Each lifestyle is surrounded by an ellipse showing the 95% confidence interval around their corresponding 108 monthly samples. Red circles represent all monthly samples from the three HMA hosts, and green diamonds denote all monthly samples belonging to the three LMA hosts. ANOSIM: R=0.268, P<0.001.

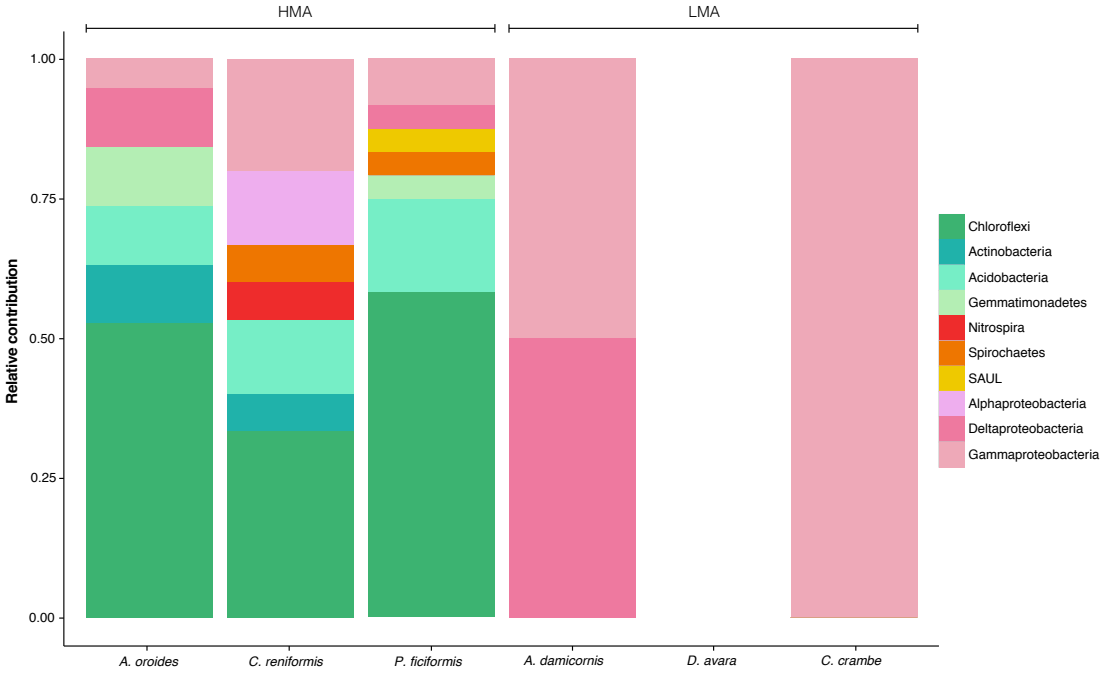

Figure S2: Taxonomic profiles of core microbiomes across hosts. Taxonomic classification at the phylum level of core taxa assigning to sponge-specific clusters and their relative contribution to species richness for each core microbiome.

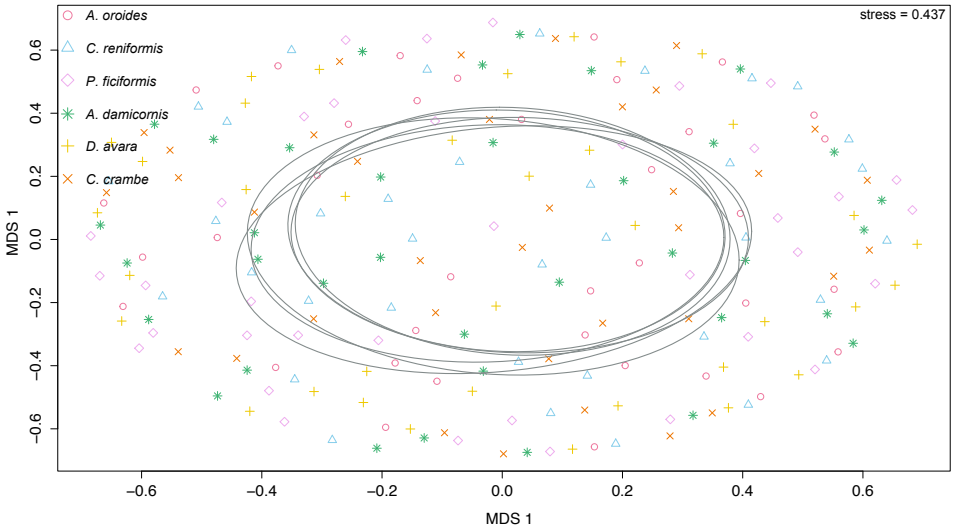

Figure S3: Microbiome compositional similarity across hosts' "stochastic realization". Non-metric multidimensional scaling (NMDS) calculated on the average Jaccard distances between monthly samples for each hosts' "stochastic realization". The average distance was calculated from 999 permutations of the null model for each host. ANOSIM: R=-0.017, P=1. See *Null model* in the *Methods* section for more details.

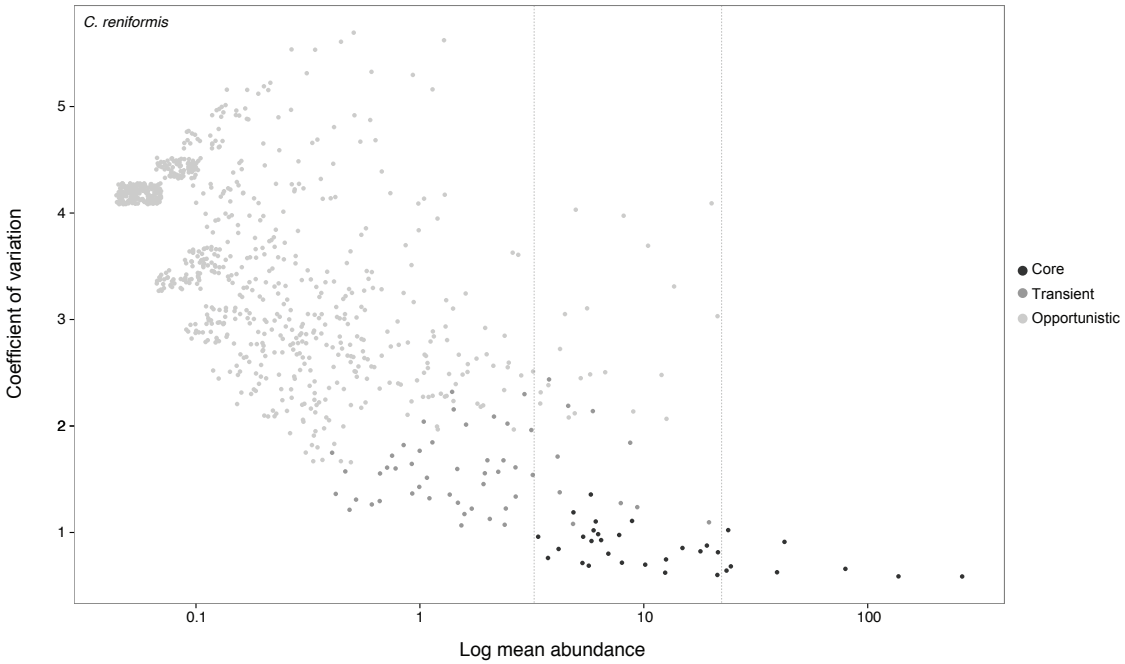

Figure S4: Abundance-stability relationship across microbiomes and hosts. The relationship between coefficient of variation (CV) and the (log) mean abundance of individual taxa for host *C. reniformis*. Overlaying points have been separated by adding jitter (random noise) of 0.1 in both y and x direction. Opportunistic, transient and core taxa are each shown by an increasing grey scale (light-to-dark). Individual core and transient taxa are generally more stable (Kruskal-Wallis test: H =2198, df=2, P<0.001 two-tailed; Dunn's post-hoc test with bonferroni correction; P <0.001) and abundant (Kruskal-Wallis test: H =1694, df= 2, P<0.001; Dunn's post-hoc test with bonferroni correction; P< 0.001 two-tailed) than opportunistic taxa. The gray dashed vertical lines mark a potentially critical area by which core microbiome temporal stability can be predicted. If there are only a few abundant and occasional taxa relative to the number of core taxa, stability is predicted to be high, whereas if there are many abundant and occasional taxa compared to the number of core taxa, stability is predicted to be low.

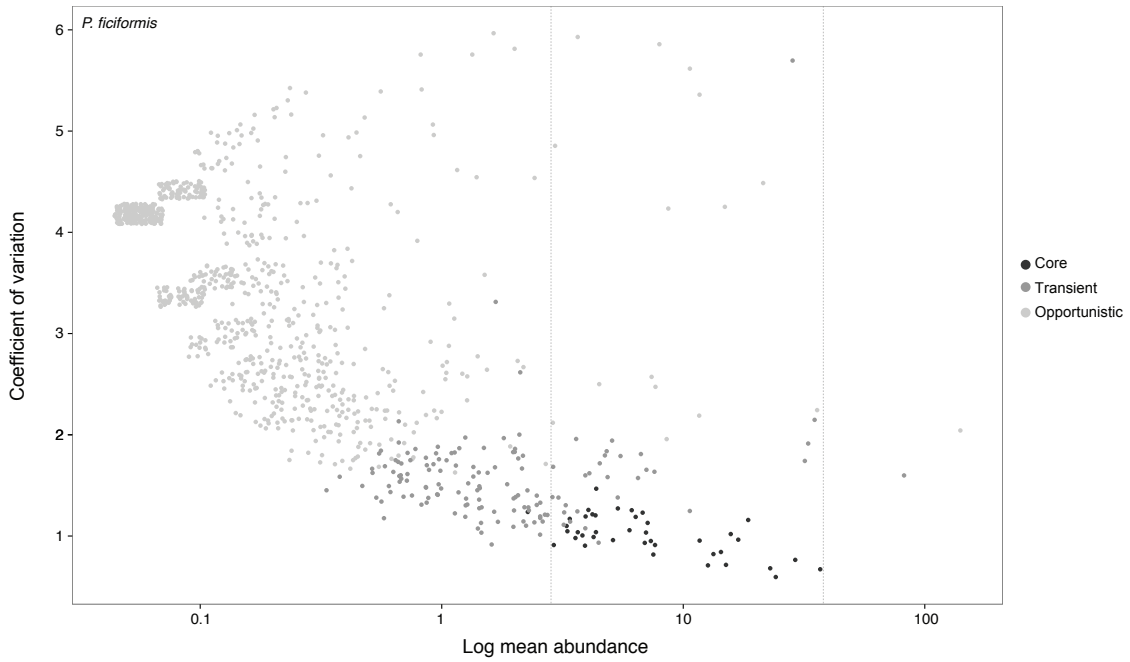

Figure S5: Abundance-stability relationship across microbiomes and hosts. The relationship between coefficient of variation (CV) and (log) mean abundance of individual taxa for host *P. ficiformis*. Overlaying points have been separated by adding jitter (random noise) of 0.1 in both y and x direction. Opportunistic, transient and core taxa are each shown by an increasing grey scale (light-to-dark). Individual core and transient taxa are generally more stable (Kruskal-Wallis test: H =2198, df=2, P<0.001 two-tailed; Dunn's post-hoc test with bonferroni correction; P <0.001) and abundant (Kruskal-Wallis test: H =1694, df= 2, P<0.001; Dunn's post-hoc test with bonferroni correction; P< 0.001 two-tailed) than opportunistic taxa. The gray dashed vertical lines mark a potentially critical area by which core microbiome temporal stability can be predicted.. If there are only a few abundant and occasional taxa relative to the number of core taxa, stability is predicted to be high, whereas if there are many abundant and occasional taxa compared to the number of core taxa, stability is predicted to be low.

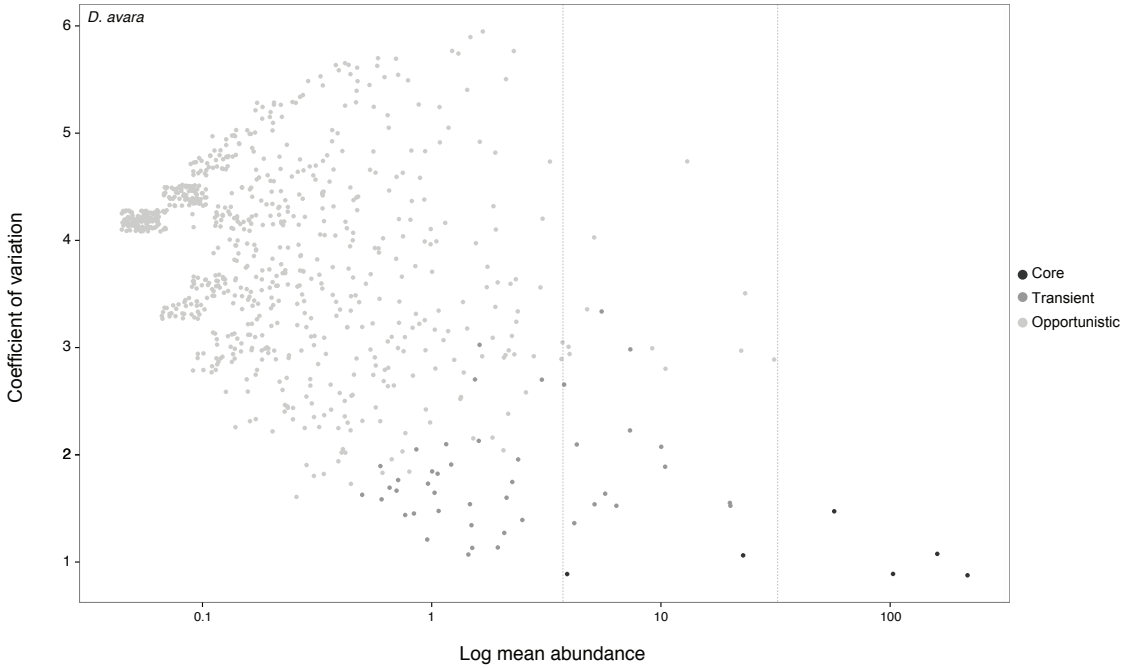

Figure S6: Abundance-stability relationship across microbiomes and hosts. The relationship between coefficient of variation (CV) and (log) mean abundance of individual taxa for host *D. avara*. Overlaying points have been separated by adding jitter (random noise) of 0.1 in both y and x direction. Opportunistic, transient and core taxa are each shown by an increasing grey scale (light-to-dark). Individual core and transient taxa are generally more stable (Kruskal-Wallis test: H =2198, df=2, P<0.001 two-tailed; Dunn's post-hoc test with bonferroni correction; P <0.001) and abundant (Kruskal-Wallis test: H =1694, df= 2, P<0.001; Dunn's post-hoc test with bonferroni correction; P< 0.001 two-tailed) than opportunistic taxa. The gray dashed vertical lines mark a potentially critical area by which core microbiome temporal stability can be predicted. If there are only a few abundant and occasional taxa relative to the number of core taxa, stability is predicted to be high, whereas if there are many abundant and occasional taxa compared to the number of core taxa, stability is predicted to be low.

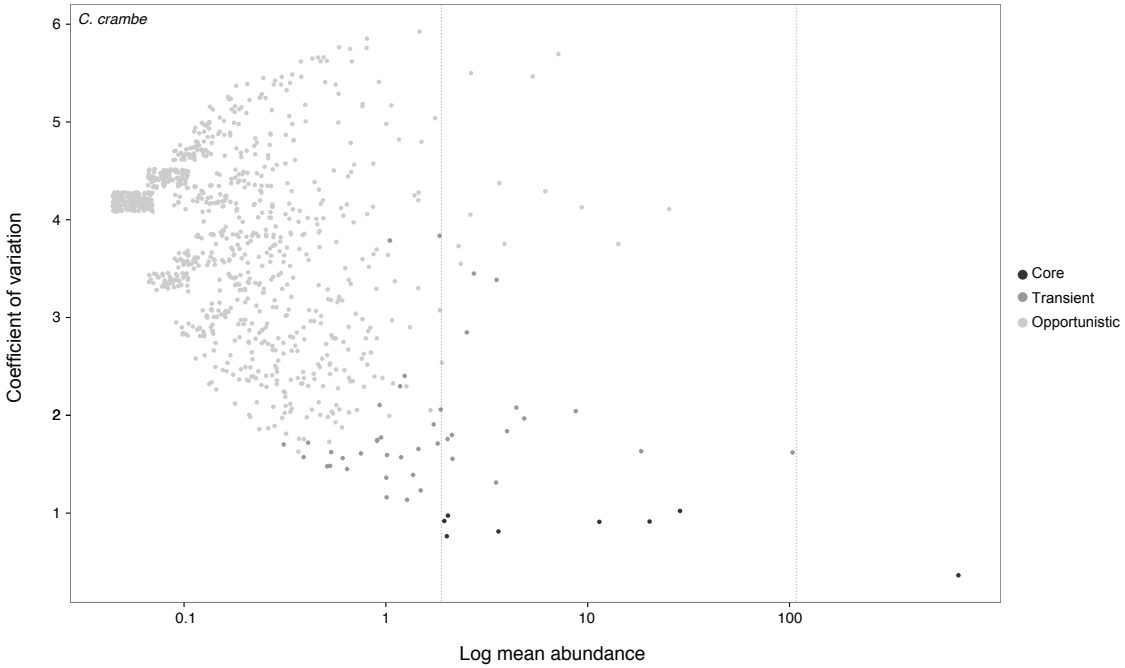

Figure S7: Abundance-stability relationship across microbiomes and hosts. The relationship between coefficient of variation (CV) and (log) mean abundance of individual taxa for host *C. crambe*. Overlaying points have been separated by adding jitter (random noise) of 0.1 in both y and x direction. Opportunistic, transient and core taxa are each shown by an increasing grey scale (light-to-dark). Individual core and transient taxa are generally more stable (Kruskal-Wallis test: H =2198, df=2, P<0.001 two-tailed; Dunn's post-hoc test with bonferroni correction; P <0.001) and abundant (Kruskal-Wallis test: H =1694, df= 2, P<0.001; Dunn's post-hoc test with bonferroni correction; P< 0.001 two-tailed) than opportunistic taxa. The red dashed lines mark a potentially critical area by which core microbiome temporal stability can be predicted. If there are only a few abundant and occasional taxa relative to the number of core taxa, stability is predicted to be high, whereas if there are many abundant and occasional taxa compared to the number of core taxa, stability is predicted to be low.

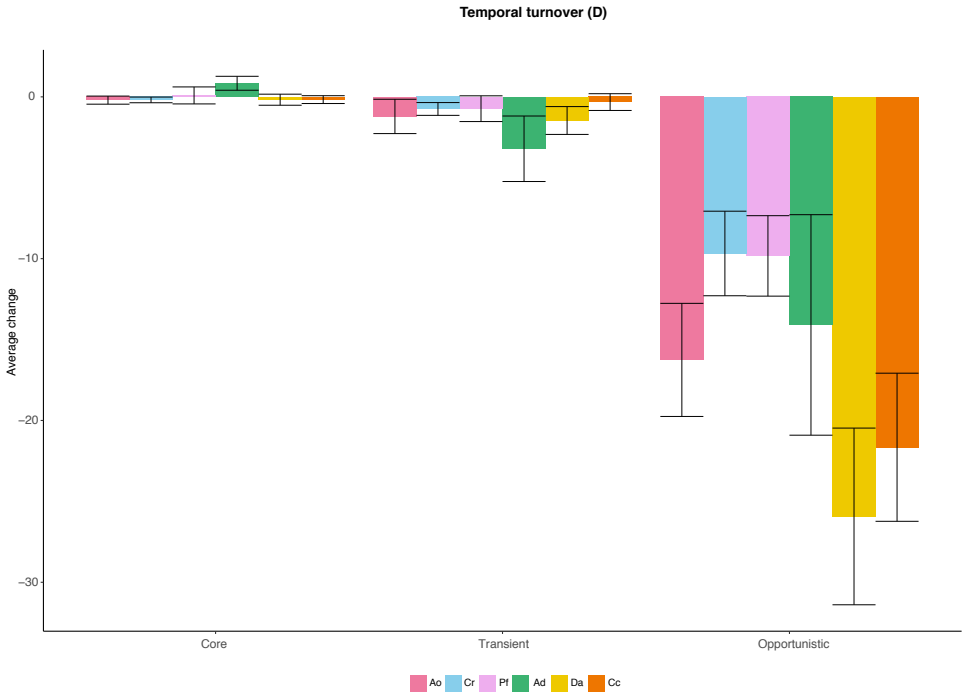

Figure S8: Temporal turnover for each assemblage and host. Total temporal turnover (D) for for each assemblage and host. Colors denote host species. Red: *A. oroides*, blue: *C. reniformis*, pink: *P. ficiformis*, green: *A. damicornis*, yellow: *D. avara*, and orange: *C. crambe*.

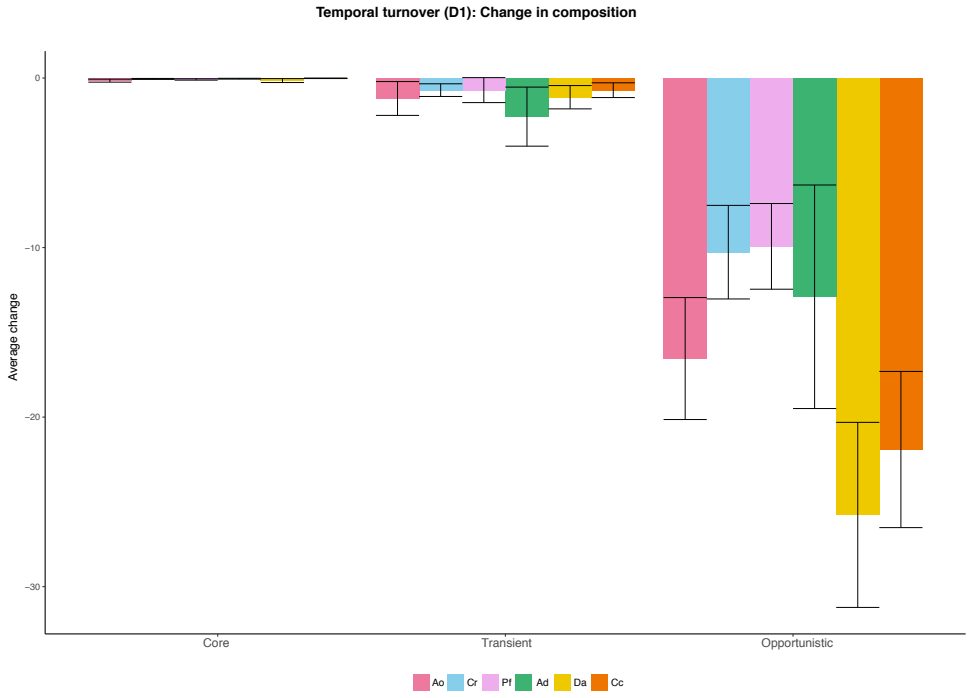

Figure S9: Temporal turnover for each assemblage and host. Temporal turnover in terms of species composition ($D1$) for for each assemblage and host. Colors denote host species. Red: *A. oroides*, blue: *C. reniformis*, pink: *P. ficiformis*, green: *A. damicornis*, yellow: *D. avara*, and orange: *C. crambe*. Transient and opportunistic assemblages were mainly governed by changes in microbial composition (Mann-Whitney U-Test: U=10223, P<0.001 two-tailed; Mann-Whitney U-Test: U=696, P<0.001 two-tailed, respectively). See *Methods* section for detailed information.

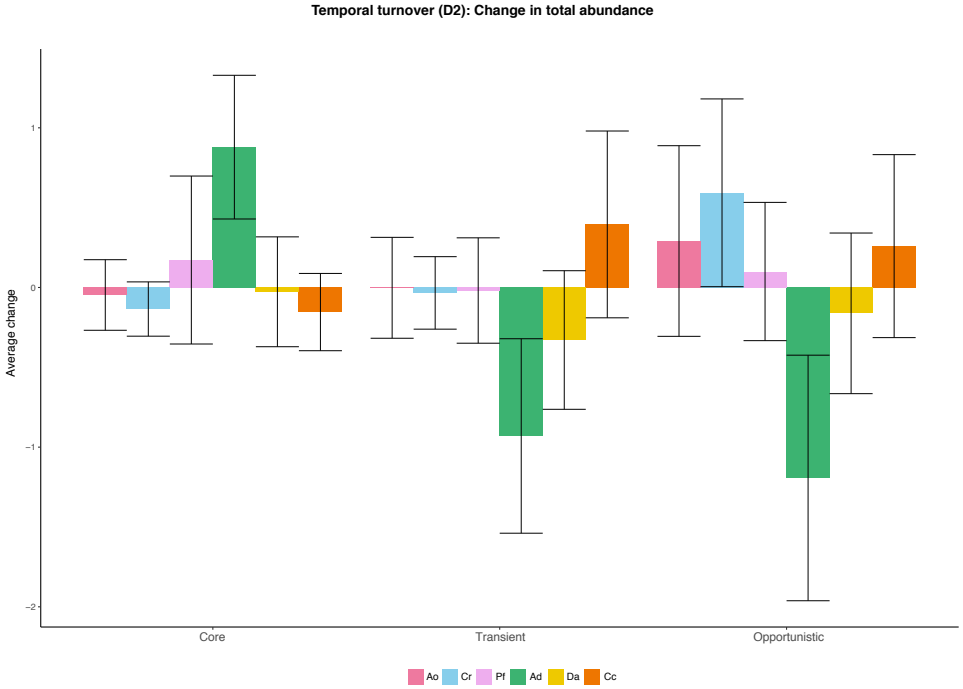

Figure S10: Temporal turnover for each assemblage and host. Temporal turnover in terms of total abundance ($D2$) for for each assemblage and host. Colors denote host species. Red: *A. oroides*, blue: *C. reniformis*, pink: *P. ficiformis*, green: *A. damicornis*, yellow: *D. avara*, and orange: *C. crambe*. Core microbiomes were overall driven by changes in abundance (Mann-Whitney U-Test: U=16676, P<0.001 two-tailed). See *Methods* section for detailed information.

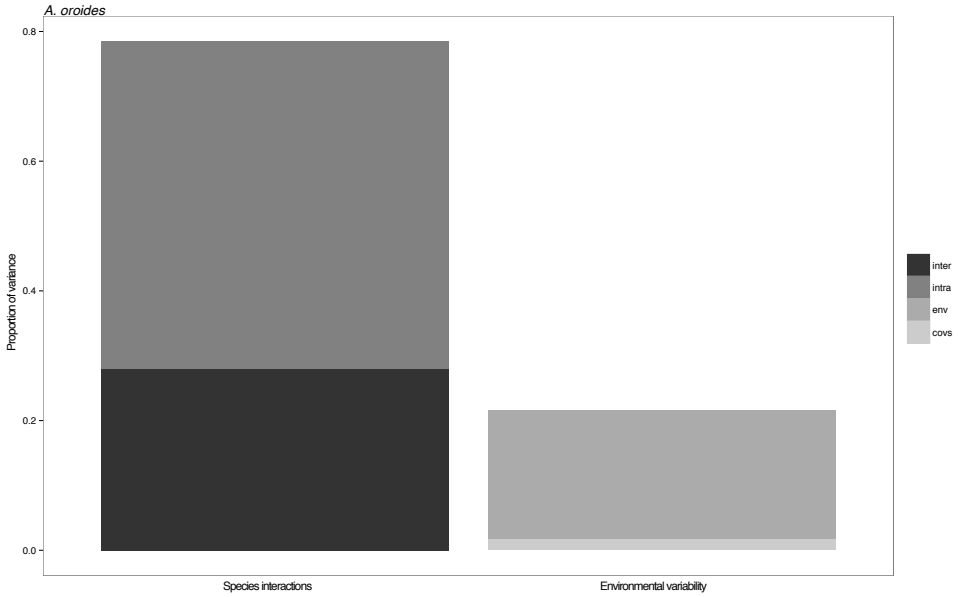

Figure S11: Processes explaining temporal variation in core microbial population abundances across hosts. Proportion of variance explained by species interactions (i.e., inter- and intreaspecific interactions) and environmental variability (i.e., variance explained by the included covariates and residual environmental variability) for host *A. oroides*. Colors are in gray scale from interspecific interactions (darkest) to variance explained by covariates (lightest).

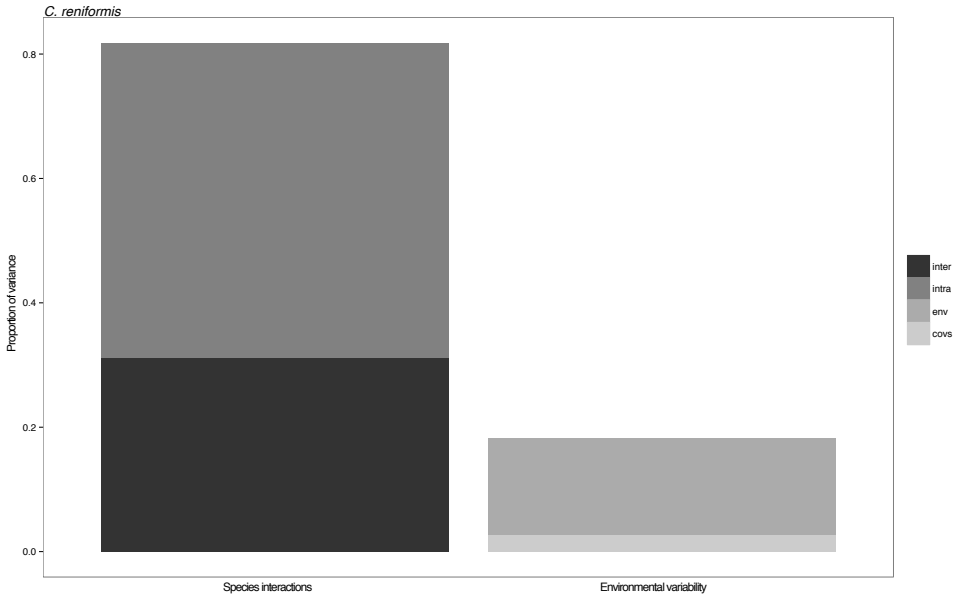

Figure S12: Processes explaining temporal variation in core microbial population abundances across hosts. Proportion of variance explained by species interactions (i.e., inter- and intreaspecific interactions) and environmental variability (i.e., variance explained by the included covariates and residual environmental variability) for host *C. reniformis*. Colors are in gray scale from interspecific interactions (darkest) to variance explained by covariates (lightest).

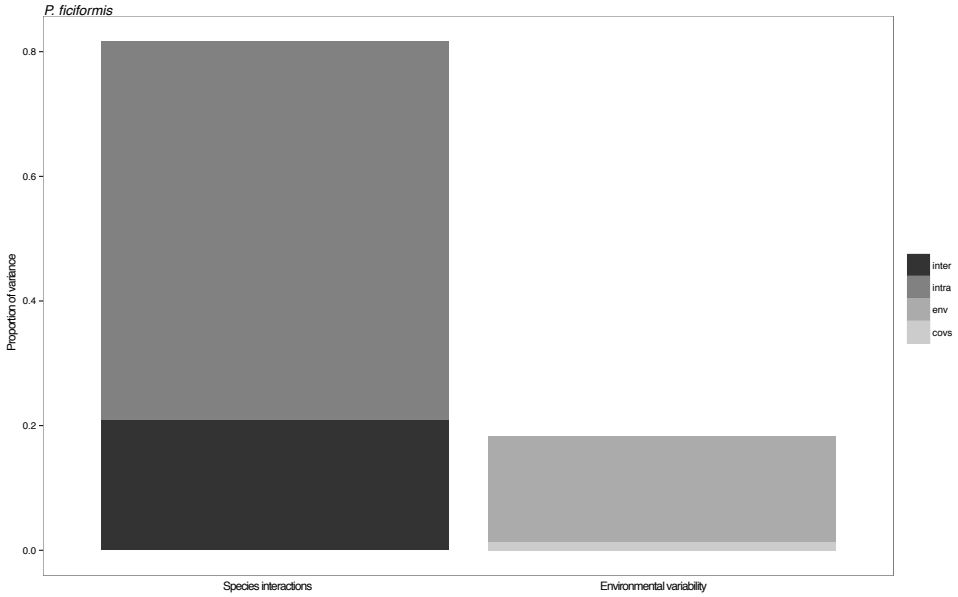

Figure S13: Processes explaining temporal variation in core microbial population abundances across hosts. Proportion of variance explained by species interactions (i.e., inter- and intreaspecific interactions) and environmental variability (i.e., variance explained by the included covariates and residual environmental variability) for host *P. ficiformis*. Colors are in gray scale from interspecific interactions (darkest) to variance explained by covariates (lightest).

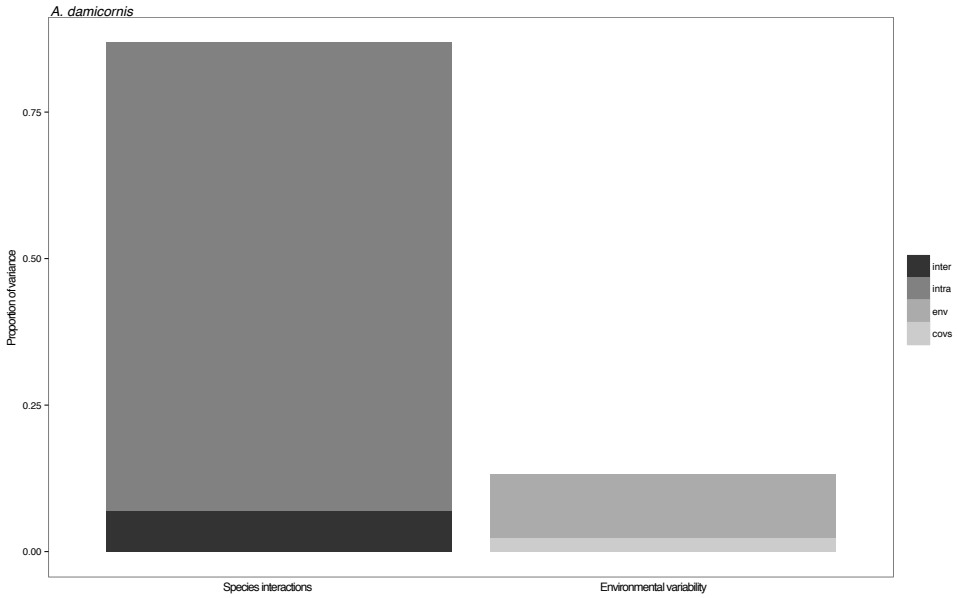

Figure S14: Processes explaining temporal variation in core microbial population abundances across hosts. Proportion of variance explained by species interactions (i.e., inter- and intreaspecific interactions) and environmental variability (i.e., variance explained by the included covariates and residual environmental variability) for host *A. damicornis*. Colors are in gray scale from interspecific interactions (darkest) to variance explained by covariates (lightest).

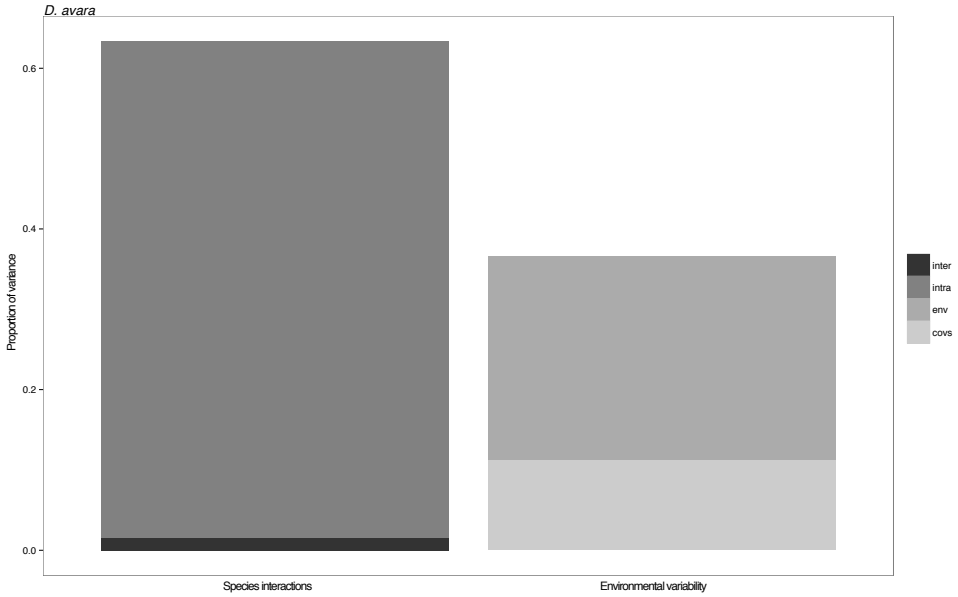

Figure S15: Processes explaining temporal variation in core microbial population abundances across hosts. Proportion of variance explained by species interactions (i.e., inter- and intreaspecific interactions) and environmental variability (i.e., variance explained by the included covariates and residual environmental variability) for host *D. avara*. Colors are in gray scale from interspecific interactions (darkest) to variance explained by covariates (lightest).

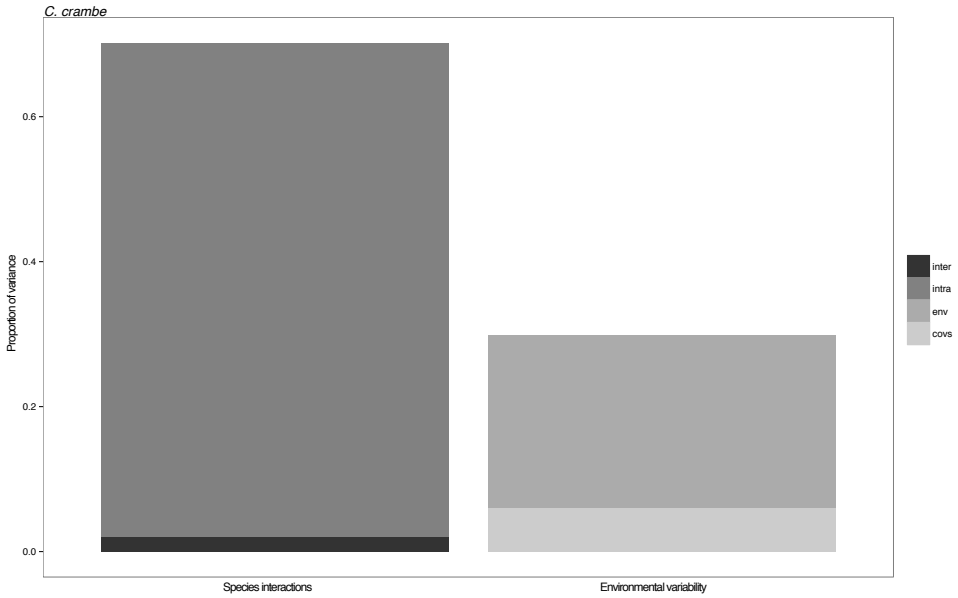

Figure S16: Processes explaining temporal variation in core microbial population abundances across hosts. Proportion of variance explained by species interactions (i.e., inter- and intreaspecific interactions) and environmental variability (i.e., variance explained by the included covariates and residual environmental variability) for host *C. crambe*. Colors are in gray scale from interspecific interactions (darkest) to variance explained by covariates (lightest).

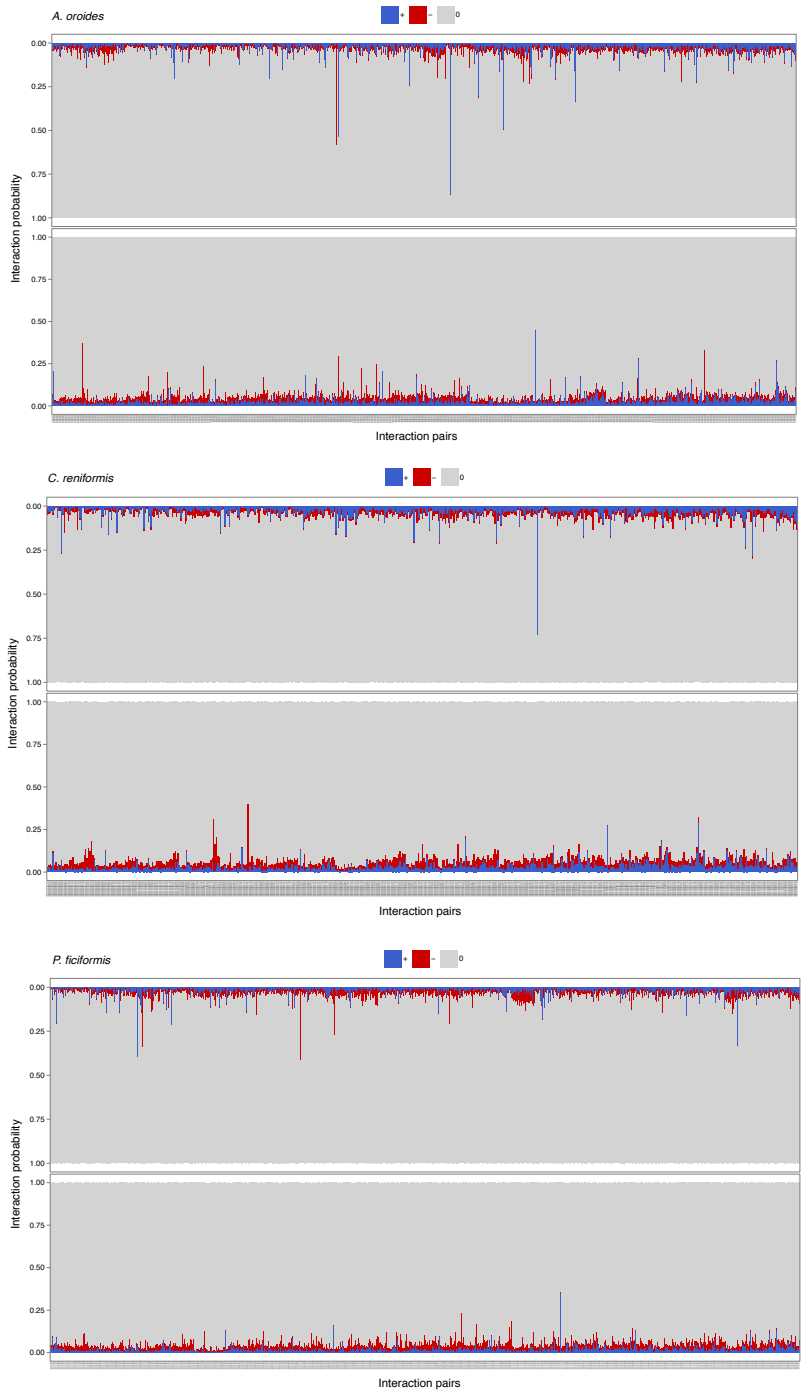

Figure S17: Interaction probabilities across HMA core microbiomes. The probability of all possible interactions within each core microbiome belonging to the HMA hosts. This was calculated from the posterior distribution of the interaction matrix $\alpha_{i,j}$ (*Equation 9* in the *Methods* section). The two y-axes show the probability for species j to interact with species i and vice versa. The x-axis displays all possible pairwise interactions. Blue and red color denote the probability for positive (blue) and negative (red) interactions. Gray depicts the remaining zero probability. Note that an interaction can have a certain probability of being both positive and negative.

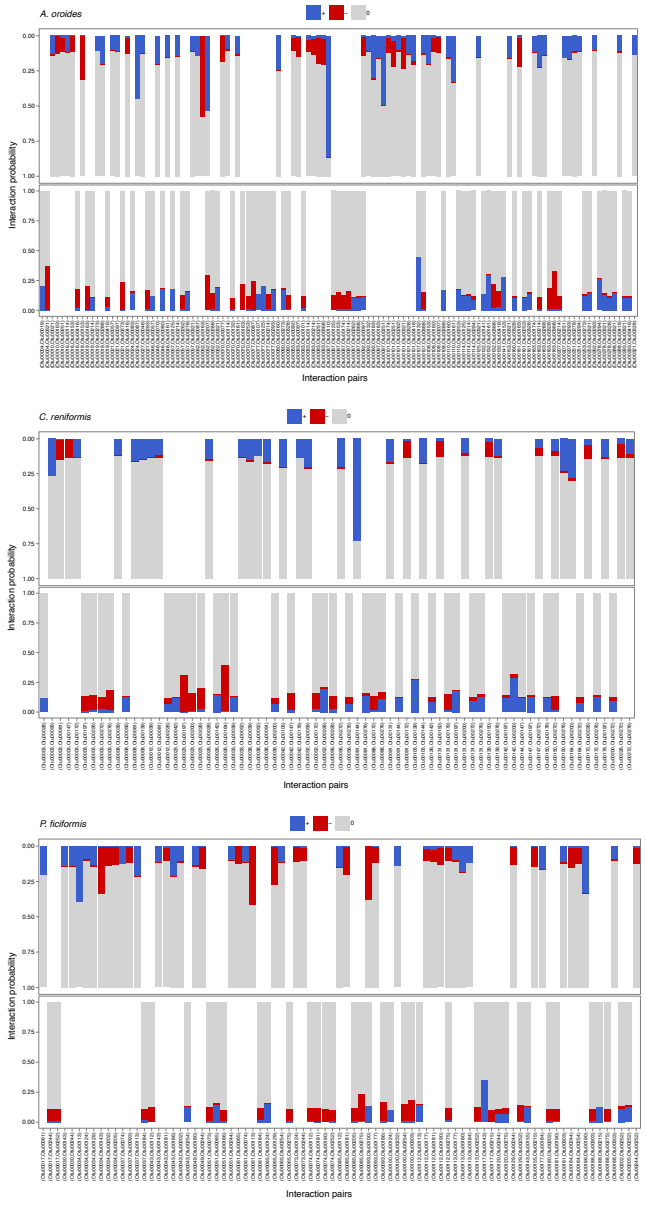

Figure S18: The most probable interactions within the HMA core microbiomes. A subset of the most probable interactions shown in Figure S17. The number of interactions corresponds to the posterior average number of links with the highest probability for each HMA core microbiome. The two y-axes show the probability for species j to interact with species i and vice versa. The x-axis displays all possible pairwise interactions. Blue and red color denote the probability for positive (blue) and negative (red) interactions. Gray depicts the remaining zero probability. Note that an interaction can have a certain probability of being both positive and negative.

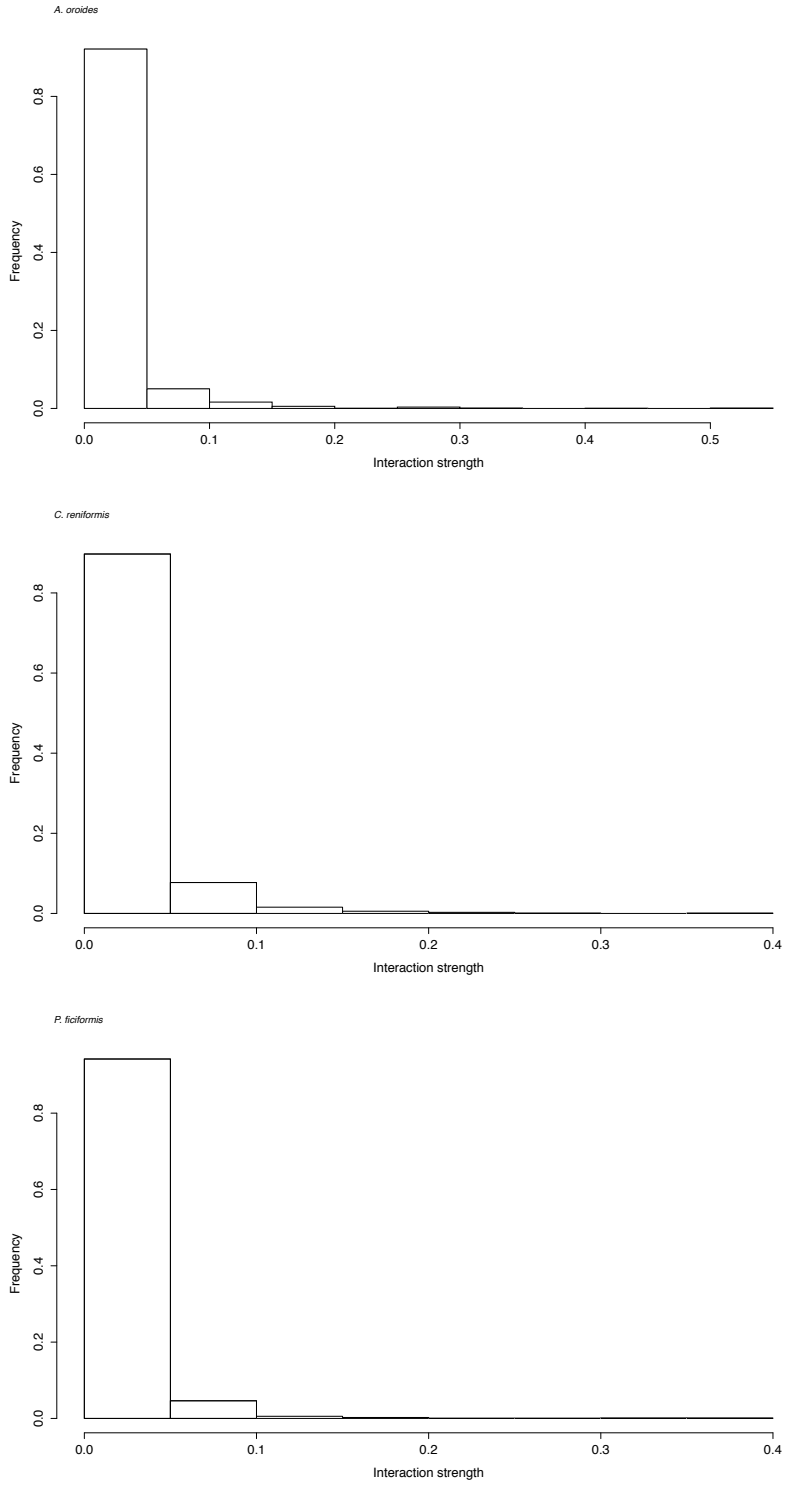

Figure S19: Frequency histogram of interaction strengths for the core microbiome belonging to the HMA hosts. Interaction strength was calculated from the posterior distribution of the interaction matrix $\alpha_{i,j}$. The distribution is skewed towards many weak and a few strong interactions.

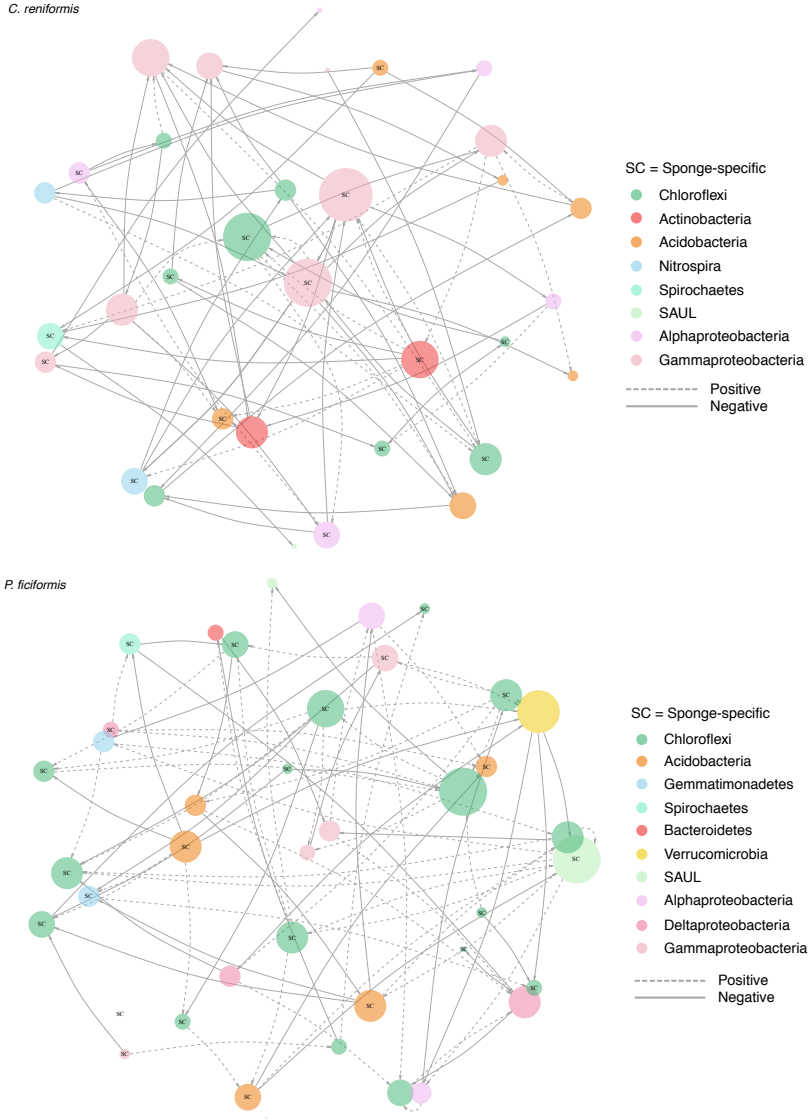

Figure S20: The core microbiome network for HMA hosts *C. reniformis* and *P. ficiformis*. Nodes represent core taxa and links their inferred ecological interactions. Node size is scaled to their degree (i.e. in and out-going links). Colors correspond to different bacterial phyla and dash and solid lines represent positive and negative interactions, respectively. Nodes marked with SC correspond to taxa assigning to sponge-specific clusters.